

**STUDY AND PREDICTION OF ELECTROSPINNING
PARAMETERS FOR NANOFIBERS PRODUCTION
USING CONVOLUTIONAL NEURAL NETWORKS
CLASSIFICATION**



**A Thesis Submitted in Partial Fulfilment of the Requirement for the
Degree of Master of Science in Physics
Suranaree University of Technology
Academic Year 2020**

การศึกษาและคาดการณ์ของพารามิเตอร์ทางอิเล็กทรอนิกส์ป็นนึ่งสำหรับการผลิต
เส้นใยนาโนโดยใช้การจำแนกประเภทโครงข่ายประสาทแบบคอนโวลูชัน



วิทยานิพนธ์นี้เป็นส่วนหนึ่งของการศึกษาตามหลักสูตรปริญญาวิทยาศาสตรมหาบัณฑิต

สาขาวิชาฟิสิกส์

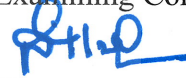
มหาวิทยาลัยเทคโนโลยีสุรนารี

ปีการศึกษา 2563

**STUDY AND PREDICTION OF ELECTROSPINNING
PARAMETERS FOR NANOFIBERS PRODUCTION USING
CONVOLUTIONAL NEURAL NETWORKS CLASSIFICATION**

Suranaree University of Technology has approved this project submitted in partial fulfillment of the requirements for a Master's degree.

Thesis Examining Committee



(Prof. Dr. Santi Maensiri)

Chairperson



(Assoc. Prof. Dr. Sayan Kaennakham)

Member



(Dr. Wiwat Nuansing)

Member (Thesis Advisor)



(Dr. Ittipon Fongkaew)

Member (Thesis Co-Advisor)



(Dr. Phakhananan Pakawanit)

Member



(Assoc. Prof. Dr. Chatchai Jothityangkoon)

Vice Rector for Academic Affairs

and Quality Assurance

Dean of Institute of Science

ญานวรุตม์ สร้อยเงิน : การศึกษาและคาดการณ์ของพารามิเตอร์ทางอิเล็กทรอนิกส์โทรสปีนนิ่ง
สำหรับการผลิตเส้นใยนาโนโดยใช้การจำแนกประเภทโครงข่ายประสาทแบบคอนโวลูชัน
(STUDY AND PREDICTION OF ELECTROSPINNING PARAMETERS FOR
NANOFIBERS PRODUCTION USING CONVOLUTIONAL NEURAL NETWORKS
CLASSIFICATION) อาจารย์ที่ปรึกษา : อาจารย์ ดร.วิวัฒน์ นวลสิงห์, 90 หน้า.

การปั่นเส้นใยด้วยไฟฟ้าสถิตได้รับการศึกษาอย่างกว้างขวางและประยุกต์ใช้กับงานหลายประเภท ไม่ว่าจะเป็นโครงข่ายเซลล์ในวิศวกรรมเนื้อเยื่อและชีวการแพทย์ ด้วยการควบคุมพารามิเตอร์ของอิเล็กทรอนิกส์โทรสปีนนิ่งสามารถสร้างเส้นใยระดับไมโครเมตรถึงนาโนเมตรได้ ในการวิจัยนี้อิทธิพลของพารามิเตอร์ทางอิเล็กทรอนิกส์โทรสปีนนิ่งได้ถูกศึกษาว่าส่งผลต่อความเสถียรและรูปร่างของกรวยทึบเลอว์อย่างไร ในการวิจัยนี้ได้เลือกใช้สารละลายพอลิเอทิลีนออกไซด์ และพารามิเตอร์ทางอิเล็กทรอนิกส์โทรสปีนนิ่งประกอบด้วย อัตราการไหล ระยะทางจากปลายเข็มถึงตัวเก็บเส้นใย และแรงดันไฟฟ้า กระบวนการผลิตเส้นใยจะถูกควบคุมให้เกิดขึ้นภายใต้เงื่อนไขต่าง ๆ แล้วใช้กล้องวิดีโอบันทึกบริเวณปลายเข็ม ซึ่งสารละลายจะถูกดันออกมาพร้อมกับผลจากแรงทางไฟฟ้า ส่งผลให้สารละลายที่ปลายเข็มมีรูปร่างเป็นกรวยทึบเลอว์ แล้วแยกออกเป็นลำสารละลาย (เจ็ต) จากนั้นจึงยืดออกเป็นเส้นใยขนาดเล็กที่สุดในที่สุด ผลการทดลองที่บันทึกและวิเคราะห์ถูกนำมาใช้ในการฝึกสอนด้วยวิธีการเรียนรู้เชิงลึกเพื่อติดตามการเปลี่ยนแปลงของกรวยทึบเลอว์ และลำของสารละลายพอลิเมอร์ รวมทั้งระบุรูปร่างของหยดสารละลายที่ปลายเข็ม เพื่อวิเคราะห์สภาวะที่เหมาะสมสำหรับการผลิตเส้นใยให้เกิดอย่างต่อเนื่อง

จากผลการวิจัยพบว่า ความสัมพันธ์ของพารามิเตอร์อิเล็กทรอนิกส์โทรสปีนนิ่งนำไปสู่การทำนายและเพิ่มประสิทธิภาพของเทคนิคอิเล็กทรอนิกส์โทรสปีนนิ่งได้ ในส่วนของการติดตามการเปลี่ยนแปลงของกรวยทึบเลอว์และลำของสารละลายพอลิเมอร์ ทำให้ทราบความสัมพันธ์ของอัตราการไหล ระยะทางจากปลายเข็มถึงตัวเก็บเส้นใย และแรงดันไฟฟ้า ที่สามารถทำให้การผลิตเส้นใยเกิดอย่างต่อเนื่องได้ สำหรับการระบุรูปร่างของหยดสารละลายที่ปลายเข็ม พบว่า จำแนกรูปร่างได้เป็น 4 รูปแบบ ได้แก่ แบบหยด แบบหยด-เจ็ต แบบกรวย-เจ็ต และแบบหมุน นอกจากนี้ ยังพบว่ารูปร่างทั้ง 4 แบบ สามารถนำไปทำนายและกำหนดขอบเขตของพารามิเตอร์ที่เหมาะสมสำหรับผลิตเส้นใย

ให้เกิดอย่างต่อเนื่องได้ ซึ่งสามารถนำไปประยุกต์ใช้ในกระบวนการอิเล็กทรอนิกส์ปีนนิ่งระดับ
อุตสาหกรรมได้



สาขาวิชาฟิสิกส์
ปีการศึกษา 2563

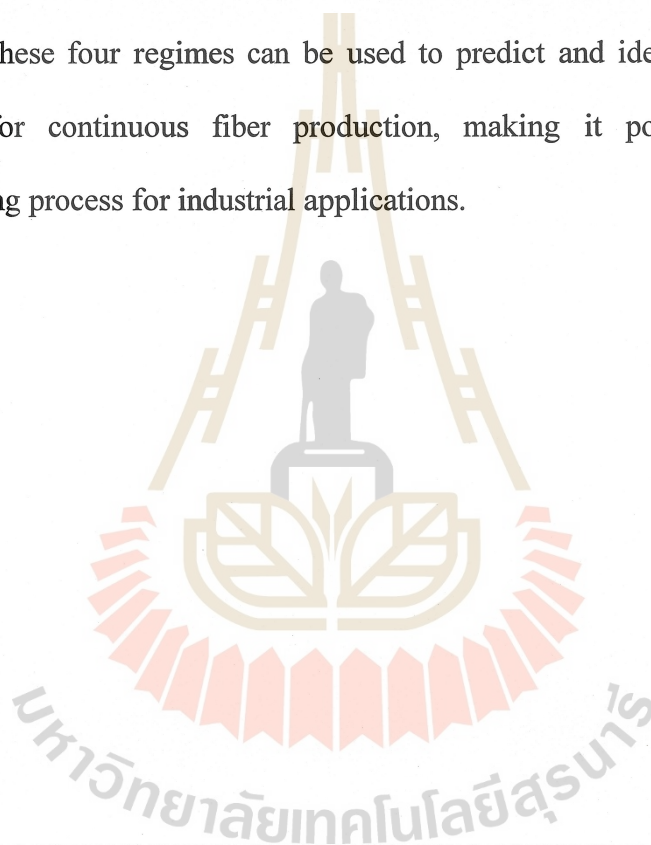
ลายมือชื่อนักศึกษา นายทศพร สิวอนเงิน
ลายมือชื่ออาจารย์ที่ปรึกษา วราณ ฐ
ลายมือชื่ออาจารย์ที่ปรึกษาร่วม อ.ดร.อ.

YANWARUTE SOI-NGOEN : STUDY AND PREDICTION OF
ELECTROSPINNING PARAMETERS FOR NANOFIBERS PRODUCTION
USING CONVOLUTIONAL NEURAL NETWORKS CLASSIFICATION.
THESIS ADVISOR : WIWAT NUANSING, Ph.D. 90 PP.

ELECTROSPINNING/TAYLOR CONE/DEEP LEARNING/POLYETHYLENE
OXIDE

Electrospun nanofibers have been widely studied and applied to many applications such as scaffold in tissue engineering and biomedical production. By controlling the electrospinning parameters, the fiber can be produced from micron-down to nano-diameters. In this work, the influence of electrospinning parameters to the stability and shape of Taylor cones was studied. A Polyethylene Oxide (PEO) aqueous solutions were electrospun under varying parameters including flow rate, tip-to-collector distance (TCD), and voltage (V). The fiber productions were controlled under various conditions and captured using a camera at the tip of the needle, where the solution is expelled because of the electric force. The resulting solution droplet at the tip of the needle was found to have the shape of a Taylor cone and was stretched into a jet of the polymer solution (jet). It was then stretched into smaller fibers eventually. The experimental results were then analyzed using a deep learning approach to track the transformation of Taylor cones, the jet of the polymer solution, and the droplet shape at the tip of the needle, with the goal of identifying the optimum conditions for continuous fiber production.

The results of this study demonstrate the correlation between electrospinning parameters and the optimization of the electrospinning process. The deep learning approach used to track the transformation of the Taylor cone and the jet of the polymer solution revealed correlations between flow rate, TCD, and voltage that are crucial for continuous fiber production. The analysis of the droplet shape at the tip of the needle revealed four distinct regimes: dripping, droplet-jet, cone-jet, and rotational. In addition, these four regimes can be used to predict and identify the appropriate parameters for continuous fiber production, making it possible to scale the electrospinning process for industrial applications.



School of Physics

Academic Year 2020

Student's Signature มาสเตอร์ รวีวัฒน์

Advisor's Signature ดร. รวีวัฒน์

Co-advisor's Signature ดร. รวีวัฒน์

ACKNOWLEDGEMENTS

For this research, it would not happen without supports from many people. Foremost, I would like to my sincere gratitude to the two project advisors, Dr. Wiwat Nuansing, who gave me the opportunity to join the research group and the inspiration for this thesis, and Dr. Ittipon Fongkaew for giving useful recommendation.

Besides my advisor, I would like to thank the rest of my thesis committee: Prof. Dr. Santi Maensiri, Assoc. Prof. Dr. Sayan Kaennakham, and Dr. Phakkhananan Pakawanit, for their attention, useful guidance, and hard questions.

Many thanks for all members in the advanced material physics research group, who give the stimulating discussions and working together. Also, I thank to Assistant Prof. Dr. Chinorat Kobdaj, Atchara Chinnakorn, Kanokpon Phumphan, QuilBot, and ChatGPT in verifying the grammar of this thesis.

I am also grateful to all beamline 1.2 members in the Synchrotron Light Research Institute (SLRI) that give me opportunity to part-time work for experience and financial support.

I would not be at this point without the support of Suranaree University of Technology and the scholarship from the Development and Promotion of Science and Technology Talents.

Finally, I would like to thank my family for their always support and encouragement.

Yanwarute Soi-ngoen

CONTENTS

	Page
ABSTRACT IN THAI.....	I
ABSTRACT IN ENGLISH	III
ACKNOWLEDGEMENTS	V
CONTENTS.....	VI
LIST OF TABLES	IX
LIST OF FIGURES	X
CHAPTER	
I INTRODUCTION.....	1
1.1 Background and motivation.....	1
1.2 Objectives of research.....	3
1.3 Scope and limitations of the study	4
1.4 Expected results	5
II LITERATURE REVIEWS	6
2.1 Electrospinning techniques	6
2.1.1 Electrospinning process	6
2.1.2 Parameters of the electrospinning.....	8
2.1.3 Taylor cone	11
2.1.4 Polymer and solvent used in electrospinning.....	14
2.2 Deep learning	14

CONTENTS (Continued)

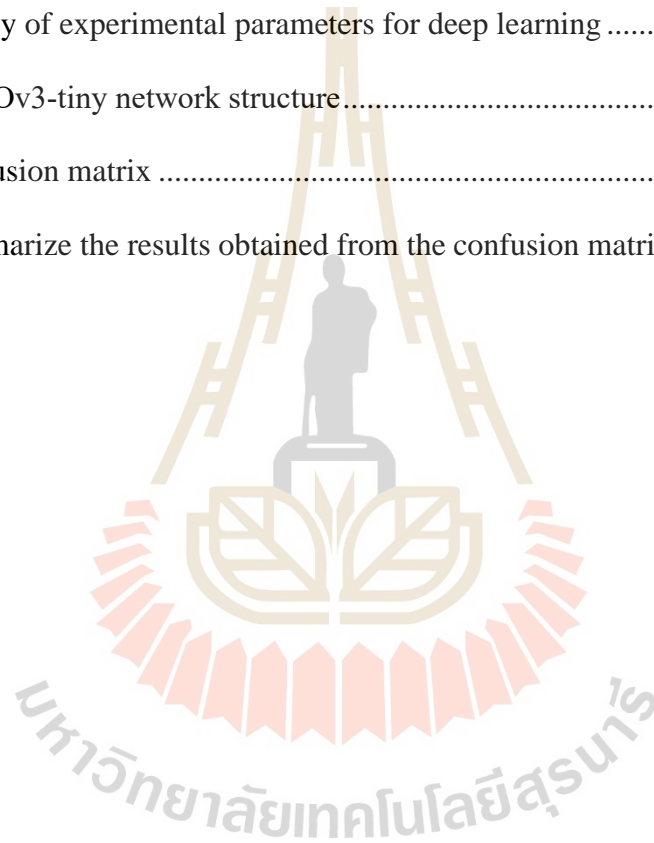
	Page
2.2.1 Convolutional neural networks.....	14
2.2.2 Artificial neural networks	18
2.3 Applied deep learning for electrospinning.....	22
2.3.1 Model application	22
2.3.2 Evaluation classification model	23
III METHODOLOGY	25
3.1 Electrospinning set-up	25
3.2 Dataset obtaining and model training	27
3.2.1 Object detection model.....	27
3.2.2 Classification model.....	31
IV RESULTS AND DISCUSSIONS	32
4.1 Result I: Model performance	32
4.1.1 Object detection model	32
4.1.2 Classification model.....	34
4.2 Result II: Correlations between flow rate and voltage.....	35
4.3 Result III: The boundary map of fabricated fibers.....	40
4.4 Result IV: Identification of regimes	42
4.5 Result V: Additional experiments and study comparisons	47

CONTENTS (Continued)

	Page
4.5.1 Continuous fabrication.....	47
4.5.2 Continuous production on regime map.....	50
4.5.3 The regime for fabricated fibers	53
V CONCLUSIONS	57
5.1 Conclusions.....	57
5.2 Recommendations.....	58
REFERENCES	59
APPENDICES	67
APPENDIX A THE BOUNDARY MAP OF FABRICATED FIBERS USING SEM FOR THE QUALITY ANALYSIS OF FIBERS.....	68
APPENDIX B A SAMPLE OF EACH CONDITION.....	70
APPENDIX C PUBLICATION AND PRESENTATIONS	81
CURRICULUM VITAE.....	90

LIST OF TABLES

Table	Page
2.1	Lists of the electrospinning parameters that influence the product 8
2.2	Survey of experimental parameters for deep learning 11
2.3	YOLOv3-tiny network structure 18
2.4	Confusion matrix 23
4.1	Summarize the results obtained from the confusion matrix 35



LIST OF FIGURES

Figure	Page
2.1	Conventional electrospinning system 7
2.2	The average diameters of the CA nanofibers (a) at TCD 12 cm (b) at TCD 18 cm by \diamond : RH 30%, \square : RH 45%, \triangle : RH 60% 9
2.3	The fiber length, average fiber diameter of PCL nanofibers versus the PCL polymer concentration 9
2.4	A schematic diagram of the droplet-jet shape showing the definition of shape feature 12
2.5	Correlations between each shape feature and fiber diameter for 6% PEO solution electrospun under 10 kV 13
2.6	Convolution calculation 15
2.7	Convolution operation (a) without padding, (b) with padding 16
2.8	Max pooling 17
2.9	Basic elements of an artificial neuron 19
2.10	Comparison of the activation function 20
2.11	(a) Architecture of a single-layer perceptron. (b) Architecture of multi-layer perceptron 22
3.1	Schematic diagram of electrospinning set-up 26
3.2	Labeling the target and contains position of the target 28
3.3	Dataset enhancements 29

LIST OF FIGURES (Continued)

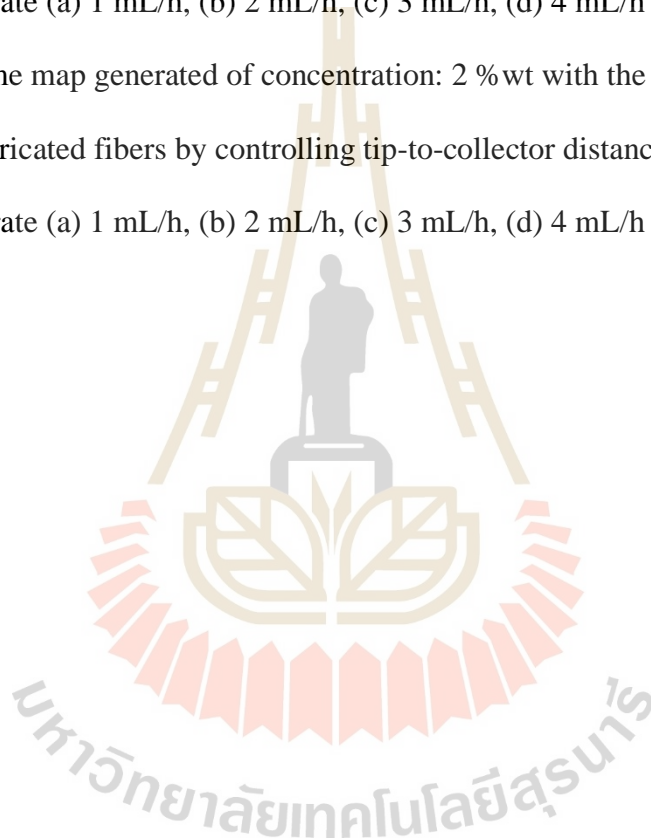
Figure	Page
3.4	Flow chart for training model 30
3.5	Example of image data from the training datasets: (a) dripping, (b) droplet-jet, (c) cone-jet, (d) rotational 31
4.1	Comparison between truth and prediction position 33
4.2	Example of Taylor cone detection 35
4.3	(a) the example graph of tracking Taylor cone on y-axis and time. (b) the example graph of tracking Taylor cone on y-axis and voltage after improvement 36
4.4	The example of analysis results at the last peak 38
4.5	Correlations between flow rate and voltage for the stable Taylor cone shapes at concentration (a) 2% wt, (b) 4% wt, and (c) 6% wt 39
4.6	The boundary map of fabricated fibers at concentration (a) 2% wt, (b) 4 % wt, and (c) 6% wt 42
4.7	Regime map generated of concentration: 2 % wt by controlling tip-to-collector distance and voltage at flow rate (a) 1 mL/h, (b) 2 mL/h, (c) 3 mL/h, (d) 4 mL/h 44
4.8	Regime map generated of concentration: 4 % wt by controlling tip-to-collector distance and voltage at flow rate (a) 1 mL/h, (b) 2 mL/h, (c) 3 mL/h, (d) 4 mL/h 45

LIST OF FIGURES (Continued)

Figure	Page
4.9	Regime map generated of concentration: 6 % wt by controlling tip-to-collector distance and voltage at flow rate (a) 1 mL/h, (b) 2 mL/h, (c) 3 mL/h, (d) 4 mL/h..... 46
4.10	The boundary map of fabricated fibers with curve of flow-in rate equal flow-out rate at concentration (a) 2 % wt, (b) 4 % wt, (c) 6 % wt..... 49
4.11	Regime map generated of concentration: 2 % wt with curve of flow-in rate equal flow-out rate by controlling tip-to-collector distance and voltage at flow rate (a) 1 mL/h, (b) 2 mL/h, (c) 3 mL/h, (d) 4 mL/h 51
4.12	Regime map generated of concentration: 4 % wt with curve of flow-in rate equal flow-out rate by controlling tip-to-collector distance and voltage at flow rate (a) 1 mL/h, (b) 2 mL/h, (c) 3 mL/h, (d) 4 mL/h 52
4.13	Regime map generated of concentration: 6 % wt with curve of flow-in rate equal flow-out rate by controlling tip-to-collector distance and voltage at flow rate (a) 1 mL/h, (b) 2 mL/h, (c) 3 mL/h, (d) 4 mL/h 53
4.14	Regime map generated of concentration: 2 % wt with the boundary map of fabricated fibers by controlling tip-to-collector distance and voltage at flow rate (a) 1 mL/h, (b) 2 mL/h, (c) 3 mL/h, (d) 4 mL/h 54

LIST OF FIGURES (Continued)

Figure	Page
4.15 Regime map generated of concentration: 4 %wt with the boundary map of fabricated fibers by controlling tip-to-collector distance and voltage at flow rate (a) 1 mL/h, (b) 2 mL/h, (c) 3 mL/h, (d) 4 mL/h	55
4.16 Regime map generated of concentration: 2 %wt with the boundary map of fabricated fibers by controlling tip-to-collector distance and voltage at flow rate (a) 1 mL/h, (b) 2 mL/h, (c) 3 mL/h, (d) 4 mL/h	56



CHAPTER I

INTRODUCTION

1.1 Background and motivation

Nowadays, fiber or fiber-like materials are widely used in daily life and tend to become more important as they are applied to other fields. Various applications of fibers have been reported in literature such as bio-sensing, drug delivery, and tissue engineering (Agrahari et al., 2017; Sasikala et al., 2019), where each fiber application needs specific properties of fiber. The fiber production method is one of the most important factors influencing fiber properties. There are several fiber production methods such as melt spinning, solution spinning, and electrospinning (Lou et al., 2020), where each method poses its advantages and disadvantages. The investigation of fiber production methods can help to improve the process and discover new products that could be used in future applications. In this study, the electrospinning technique was investigated as a method for synthesizing polymeric fibers. The electric force is utilized as the driving force for fiber production (Karimi et al., 2015). It is an effective technique for converting a large-scale process into a low-cost, broadly applicable method for fiber production on the laboratory and industrial scales (Nasouri et al., 2012; Reneker et al., 2008).

In a production process, there are many parameters that can affect the process and the product. These factors need to be controlled to have the process proceed and get the product as desired. Such a condition in the parameters is required for stable and continuous fiber production. To find out and learn more about such stable and continuous fiber production, electrospinning parameters were considered as variants for the production they involved. There are several parameters that can be developed to synthesize the desired fiber products. Joy and coworkers studied correlations between voltage and tip-to-collector distance and insights into regimes, transitions, and cone-jet shapes (Joy et al., 2021). Shin and his coworkers studied fabric nanofibers, which are produced by the droplet-jet shapes of the near-field (Shin et al., 2019). Liu and coworkers studied droplet-jet shape to predict the diameter of nanofibers (Liu et al., 2019). They considered a droplet at the tip of the needle that could regulate fiber production. However, there are many complications and a lack of investigations, and there is no feature for describing the effect of fiber production as reported in the literature. In this study, all potential parameters that may influence the production process were taken into consideration.

A good analysis method is required because several parameters are considered, which necessitates a large amount of experimental data to analyze and distinguish the contribution of each parameter. Deep learning has been the subject of numerous important and advanced research papers in recent years. It is to design and analyze algorithms that allow machines to establish rules by analyzing data automatically and using them to predict unknown data. This method can be applied to find the correlation between the electrospinning parameters and fiber production. Two

models of object detection and classification are trained for tracking the transformations of a jet or Taylor cone and classifying the Taylor cone shape using deep learning algorithms.

In summary, this study investigates the electrospinning technique with the goal of determining the conditions for stable and continuous fiber production. All potential parameters that may affect the production process are considered and deep learning is utilized for data analysis. Background on the electrospinning technique, deep learning, and its application to assist prediction and optimization of the electrospinning technique can be found in Chapter II. Electrospinning set-up and experimental plans were described, as well as the implementation of object detection and classification models, in Chapter III. In Chapter IV, the efficiency of various models is discussed, and their results are analyzed for identifying correlations between electrospinning parameters and fiber production. Conclusions regarding the significance of the findings and recommendations for further development are presented in Chapter V.

1.2 Objectives of research

The objective of this research is to use deep learning approach to improve the understanding of the electrospinning process. The specific objectives of this work are:

1.2.1 To develop tools for the analysis and interpretation of electrospinning results and production.

1.2.2 To apply deep learning techniques to identify the optimal conditions for stable and continuous fiber production.

1.2.3 To investigate the influence of various electrospinning parameters on fiber production.

1.2.4 To analyze and identify the relationship between the regime of the solution droplet at the needle tip and fiber production.

1.3 Scope and limitations of the study

The focus of this research is to understand the transformations of the solution jet during the electrospinning process and the conditions necessary for stable fiber production. The scope of this study includes:

1.3.1 Polyethylene oxide (PEO) is used as polymer for fiber fabrication through the electrospinning technique.

1.3.2 Camera (IMSHI 1600X Digital Microscope USB Endoscope Camera) is used to record the droplet at the tip of the needle.

1.3.3 The electrospun fiber morphology is observed and revealed using a scanning electron microscope (SEM).

1.3.4 Datasets from extracted videos are trained through deep learning to track the transformations of the solution jet.

1.3.5 Confusion matrix is used for evaluation and indicating the efficiency of the model.

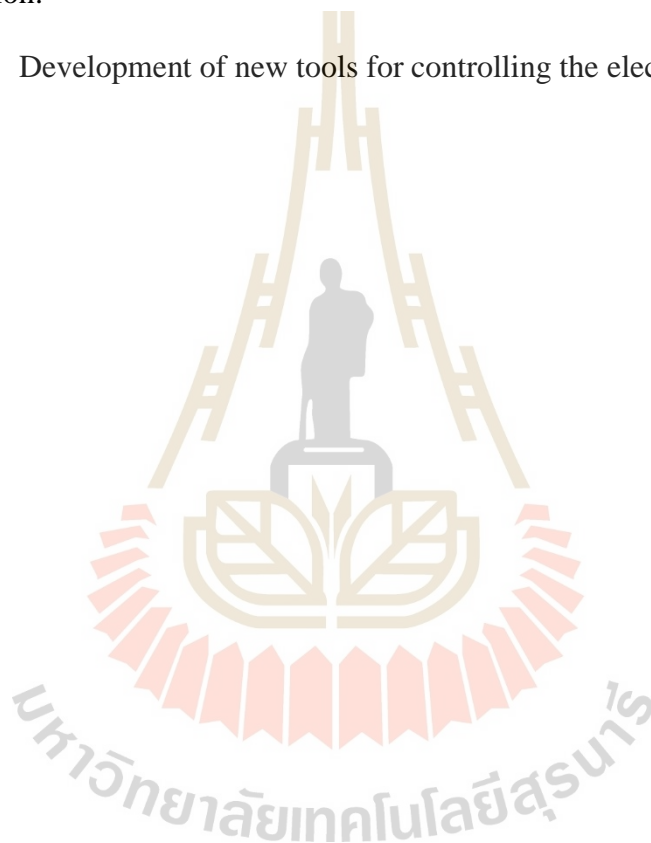
1.4 Expected results

The following are the expected outcomes of this research:

1.4.1 Accurate prediction of fiber production that can be controlled with the electrospinning parameters.

1.4.2 Improved understanding of the electrospinning parameters that impact fiber production.

1.4.3 Development of new tools for controlling the electrospinning process.



CHAPTER II

LITERATURE REVIEWS

An overview of deep learning and electrospinning is provided in this chapter. Section 2.1 explains the theoretical foundation and fascinating details of the electrospinning technology. The theoretical foundation of deep learning is presented in Section 2.2. The parameter values for steady and continuous fiber manufacturing are determined using deep learning. Section 2.3 presents the model applications for electrospinning that are carried out using deep learning. Additionally, the effectiveness of the deep learning model is assessed.

2.1 Electrospinning techniques

2.1.1 Electrospinning process

Electrospinning is an efficient technique for continuous fiber production. The technique allows the polymer solution to stretch to form fibers with micron- to nano-diameters (Karakas, 2015). In addition, the product from this technique can be applied as an additive in a wide variety of applications, such as drug delivery, tissue engineering (Alharbi et al., 2018) and filtering (Cheng et al., 2018). In this work, the main components of an electrospinning system require a high voltage supplier, a capillary tube with a pipette or syringe, a syringe pump, a needle of small diameter, and a metal collector, as shown in Figure 2.1

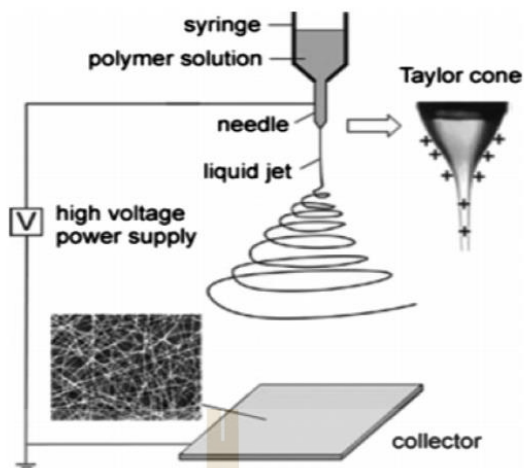


Figure 2.1 Conventional electrospinning system (Garg et al., 2011).

In the process, a polymer solution is contained in a syringe and pumped into a droplet at the tip of the needle. A high voltage is applied at the tip of the syringe's needle and the collector to create an electric field in the direction from the needle to the collector. As a result, the shape of the polymer solution droplet is distorted from a spherical to a conical shape, known as the Taylor cone (Yarin et al., 2001). As the electric field attains a critical value (V_c), the electric force on the droplet overcomes the surface tension force of the polymer solution, and thus the surface of the solution is elongated from the needle as it travels to the collector. In this process, the stretching of the jet depends on the physical characteristics of the polymer solution, and the solvent is evaporated in the air, leaving only the fibers. The fibers are collected randomly in the form of nonwoven mesh on the collector (Mottaghitlab et al., 2010; Yang et al., 2008).

2.1.2 Parameters of the electrospinning

As mentioned in Chapter I, the quality of fiber products is greatly influenced by several factors. Although there are many reports about controlling fiber production by electrospinning technique, the results of those reports do not show significant differences in the quality of the product. The reason is that there are many factors that affect the morphology or structure of the fiber products, whether known or unknown, as shown in Table 2.1.

Table 2.1 Lists of the electrospinning parameters that influence the product (Brooks et al., 2015).

Polymer	Solvent	Solution	Experimental
Molecular weight	Density	Concentration	Feed rate
Polydispersity	Zero shear viscosity	Relaxation time	Needle geometry
Intrinsic viscosity	Vapour pressure	Viscosity	Distance
Density	Dielectric constant	Vapour pressure	Voltage
Glass transition temperature	Conductivity	Conductivity	Atmospheric humidity
Dielectric constant	Dipole moment	Surface tension	Atmospheric temperature
Solubility parameters	Surface tension	Charge density	Collector geometry

From the electrospinning parameters shown in Table 2.1, it is difficult to control all parameters because some parameters have a strong influence on the product and relate to each other. Many reports have mentioned the effects of electrospinning parameters on the quality of the product. In the example, De Vrieze and his coworkers studied the effect of humidity on the cellulose acetate (CA)

nanofiber and discovered that as relative humidity (RH) increased, the average diameter of the fiber increased, as shown in Figure 2.2. (De Vrieze et al., 2009).

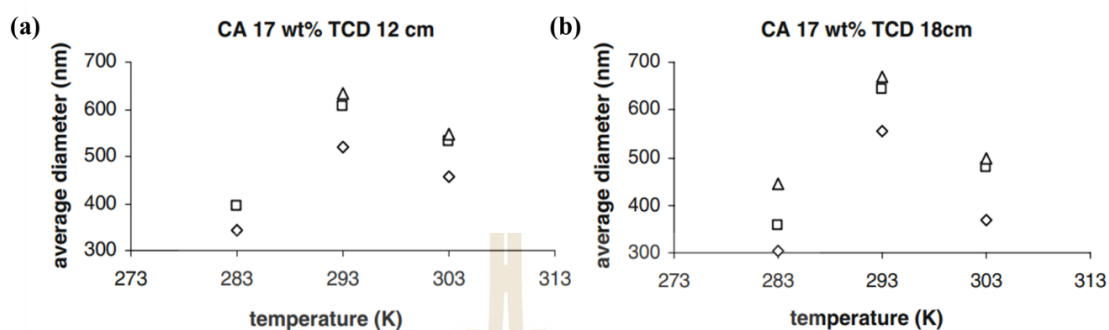


Figure 2.2 The average diameters of the CA nanofibers (a) at TCD 12 cm, (b) at TCD 18 cm. by \diamond : RH 30%, \square : RH 45%, \triangle : RH 60% (De Vrieze et al., 2009).

Beachley and his coworkers studied the effect of the polycaprolactone (PCL) polymer concentration on morphologies of fiber and found that as the PCL polymer concentration increased, length and diameter increased, as shown in Figure 2.3. (Beachley et al., 2009).

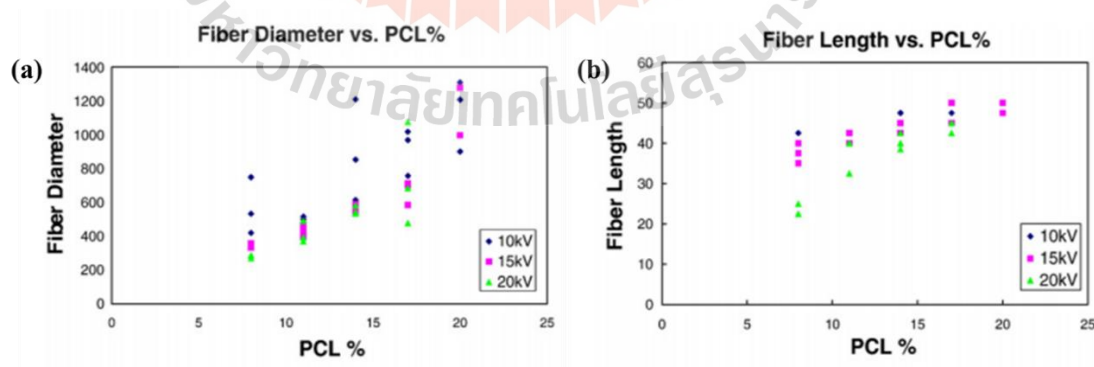


Figure 2.3 The fiber length, average fiber diameter of PCL nanofibers versus the PCL polymer concentration (Beachley et al., 2009).

There has been a lot of research on electrospinning parameters to better understand the technique, utilizing deep learning to discover the relationship between the parameters and fiber production by gathering datasets and training models with them. Table 2.2 summarizes the experimental parameters for each report. The results of the reports represent the quality of the product. These studies provide some potential insights about the correlation between the experimental data and the mean predictions by considering some parameters. However, there is no prediction that considers all the possible parameters because there are some parameters that are difficult to measure or control.

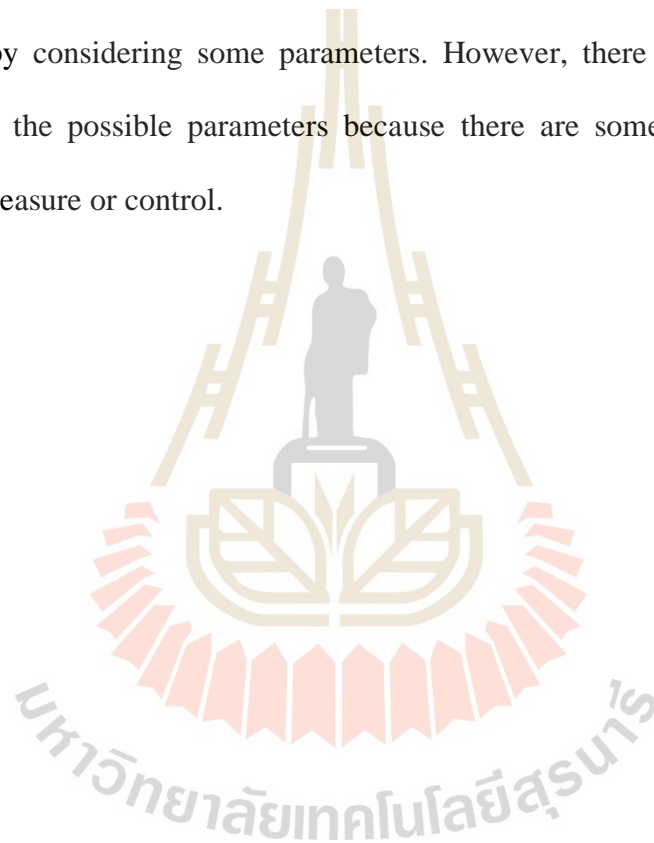


Table 2.2 Survey of experimental parameters for deep learning.

Authors	Concentration	Conductivity	Ratio of solvents	V	TCD	Flow rate	Drum speed	Temperature	Activation function
Sarkar et al. (2009)	✓	✓	×	✓	×	✓	×	×	Hyperbolic tangent
Nasouri et al. (2012)	✓	×	×	✓	✓	×	×	×	Hyperbolic tangent
Rabbi et al. (2012)	✓	×	×	✓	✓	×	×	×	Hyperbolic tangent
Khanlou et al. (2014)	✓	×	×	×	✓	✓	×	×	Sigmoid
Paskiabi et al. (2015)	✓	×	×	✓	✓	×	✓	×	Sigmoid, Linear
Karimi et al. (2015)	✓	×	×	✓	✓	×	×	✓	Sigmoid
Khatti et al. (2017)	✓	×	✓	✓	✓	×	×	×	Hyperbolic tangent, Sigmoid, Linear
Hosaini-Alvand et al. (2017)	✓	×	✓	✓	✓	×	×	×	Purelin
Ieracitano et al. (2017)	✓	×	×	✓	✓	✓	×	×	Hyperbolic tangent

*Note: V is applied voltage, TCD is Tip to Collector Distance.

2.1.3 Taylor cone

The conical surface that forms when the droplet is subjected in the electric field, referred as the Taylor cone due to charges of polymer solution is induced on the surface of the droplet by the electric field. When the electric field attains a critical

value (V_c), the droplet changes shape from spherical to conical (Garg et al., 2011). In the electrospinning process, the transformation of a jet or Taylor cone is important phase that before the droplets elongate into a straight jet. From observable features of the droplet-jet, studies conducted by Liu and Reneker provided harbinger of sophisticated process controls the behavior of the droplet-jet jets (Liu et al., 2019). There are three shape features as “L-R curvature”, “initial jet diameter”, and “transition slope”, were identified as shown in Figure 2.4. The transformation from droplet to jet is quantified by these features. Figure 2.5 shows the correlations between each shape feature and fiber diameter and provide a prediction of fiber diameter. Thus, an observable droplet at the tip of the needle is interesting for identifying features as parameters, and control of these features is possible to control the quality of the product.

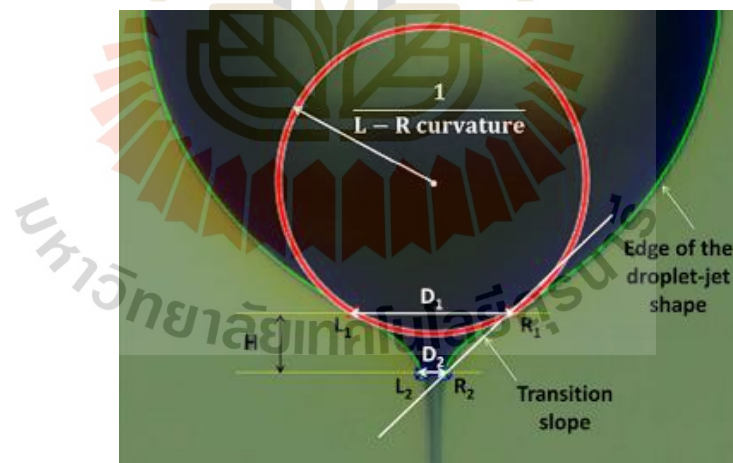


Figure 2.4 A schematic diagram of the droplet-jet shape showing the definition of shape feature (Liu et al., 2019).

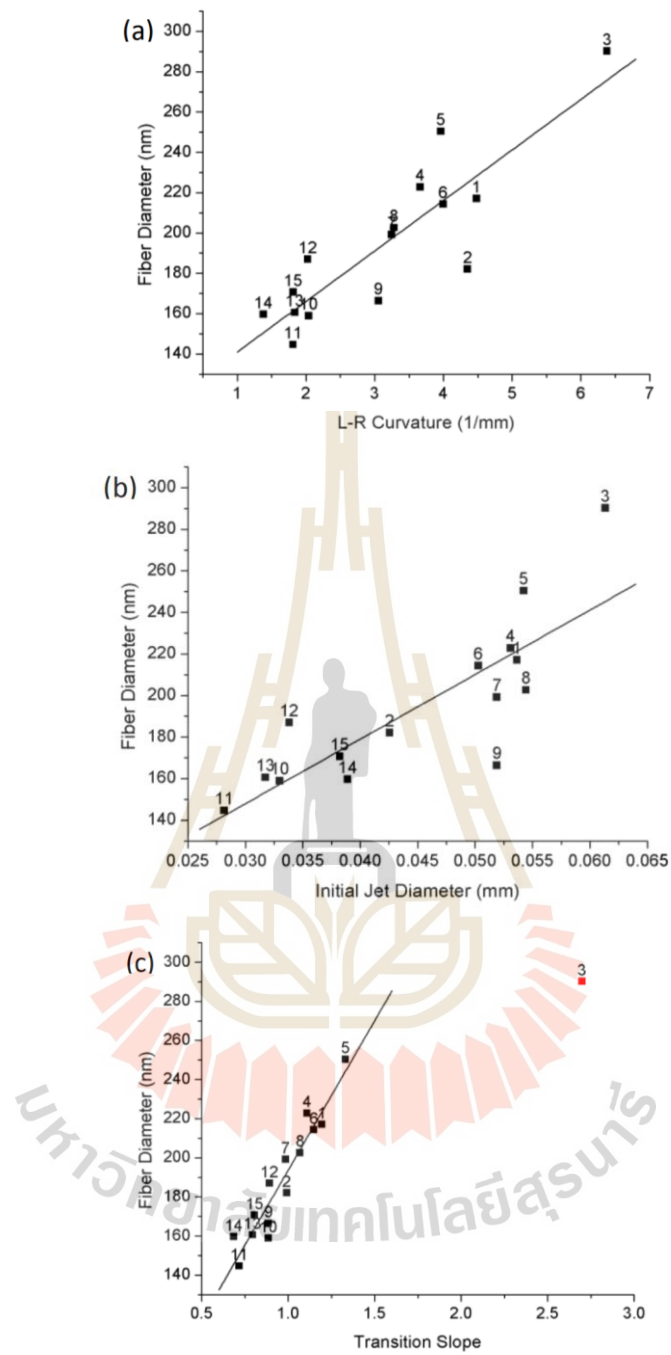


Figure 2.5 Correlations between each shape feature and fiber diameter for 6% PEO solution electrospun under 10 kV (Liu et al., 2019).

2.1.4 Polymer and solvent used for electrospinning

There are many polymers that can be technically synthesized into polymeric fibers by electrospinning. Each polymer has different properties. It is important to select polymers that suit the purpose of the work. In addition, the kinds of solvents must be used according to the kinds of polymers. In this work, polyethylene oxide (PEO) was investigated because of its biodegradability, biocompatibility, non-toxicity, and solubility in water. These properties can also be applied to PEO nanofibers in the biomedical and food industries (Filip et al., 2019). Thus, it is an easily electrospinnable solution and safe for experimentation.

2.2 Deep learning

Deep learning is a subfield of machine learning that can learn and make decisions on its own, learning from statistical knowledge in datasets through a hierarchy of features. Deep learning's architecture has a background in artificial neural networks or a functional structure that mimics the biological neural network of the human brain (Jamshidi et al., 2001).

2.2.1 Convolutional neural networks

Convolutional neural network (CNN) is a deep learning algorithm that brings a revolution in the visual regions of computers. The advantages of CNN are applications including classification, object detection, segmentation, meaning, image retrieval, and caption. The principle of CNN is feature extraction from the dataset for analysis and implement the newly obtained features in the prediction. There are three types of layers in the structure of CNN:

- Convolutional layers** consist of the input image and the convolution matrix. The input image is a digital image, and the convolution matrix is a similar filter, also known as kernel/filter. The input image is convolved with the convolution matrix. Then, the convolution matrix shifts to the right with the stride value until the entire width. After that, it shifts down with the same stride value and starts the left of the image, where this process repeats for the entire image. A new image is generated to the next layer as shown in Figure 2.6. The new image is reduced in dimensions as compared to the input image.

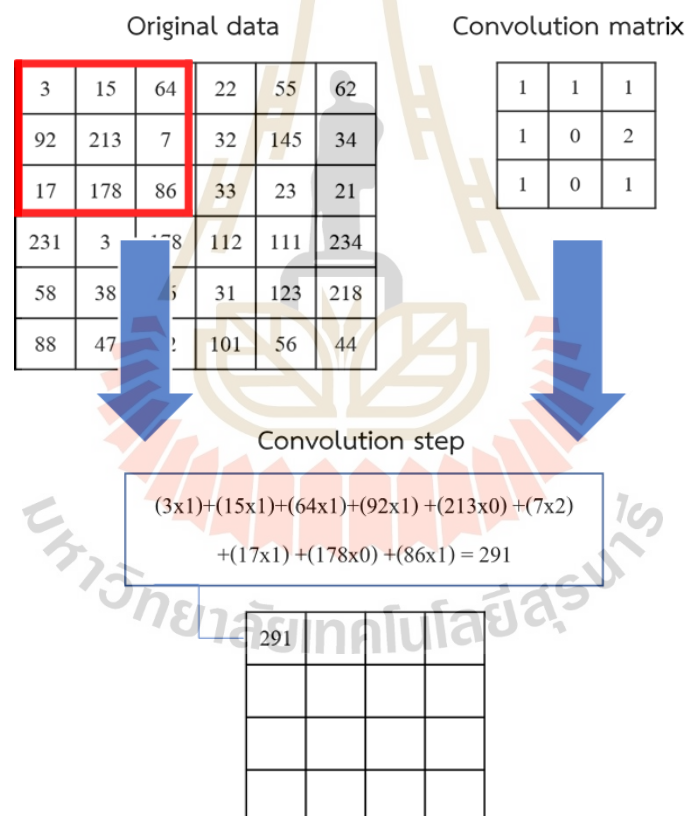


Figure 2.6 Convolution calculation.

During convolution, the dimension of the new image would decrease. To increase or remain the dimension of the new image same as the input image,

the padding is applied before convolutional process by adding zero around the edge of the input image as shown in Figure 2.7.

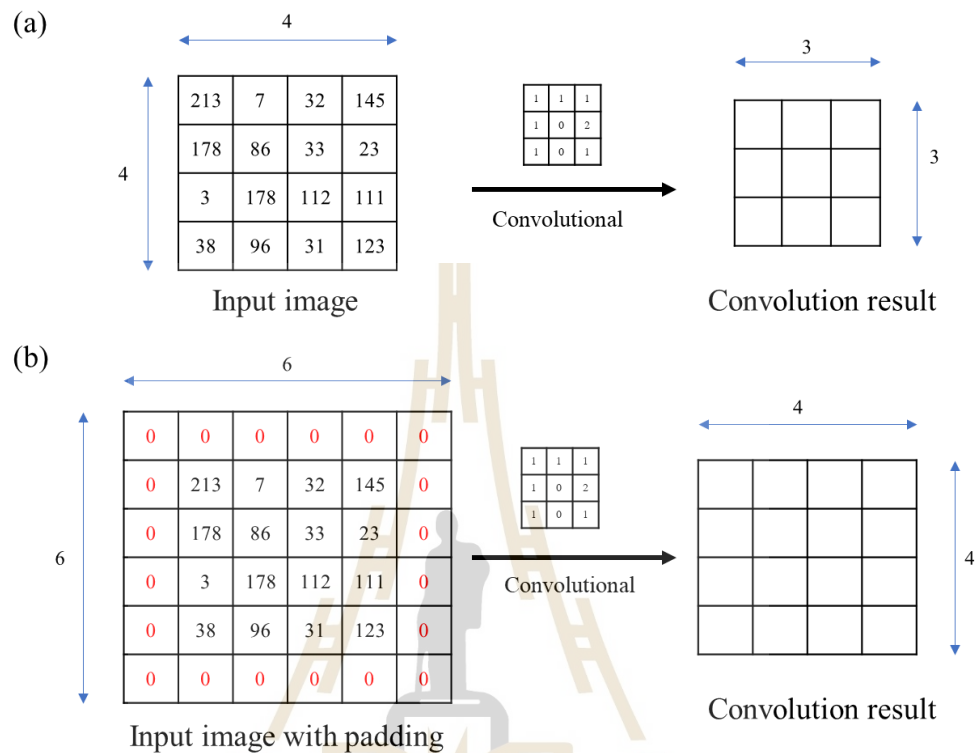


Figure 2.7 Convolution operation (a) without padding, (b) with padding.

- **The subsampling layer/ Pooling Layer** is a layer to reduce the dimensions of input image by combining among pixel blocks into a pixel block. Max pooling method is frequently used to calculate the pixel value of the output image. The maximum value of each local group is selected. Figure 2.8 shows an example of the subsampling layer with max pooling method.

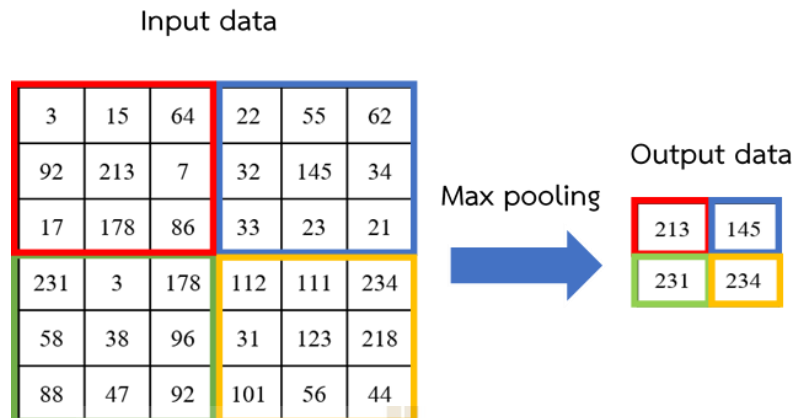


Figure 2.8 Max pooling.

- **Fully connected layer** is a layer that connects every neuron in the previous layer to every neuron in the next layer. The outputs are probabilities of each category to classify the input image.

Convolutional neural networks are used in YOLO models, which can identify multiple objects and their positions on the pixels of an image (He et al., 2019). YOLO network structure consists of convolutional layers, pooling layers and two fully connected layers. YOLOv3-tiny is an object detection algorithm that is reduced from YOLOv3 and has a smaller model size for constrained environments (Fang et al., 2020). It has a fundamental knowledge of convolutional neural networks and the network structure as shown in Table 2.3. Cira core software is used in this work because it is a program with an operating system that can create various algorithms or applications and models that are available.

Table 2.3 YOLOv3-tiny network structure (He et al., 2019).

Layer	Type	Filters	Size/Stride	Input	Output
0	Convolutional	16	$3 \times 3/1$	$416 \times 416 \times 3$	$416 \times 416 \times 16$
1	Maxpool		$2 \times 2/2$	$416 \times 416 \times 16$	$208 \times 208 \times 16$
2	Convolutional	32	$3 \times 3/1$	$208 \times 208 \times 16$	$208 \times 208 \times 32$
3	Maxpool		$2 \times 2/2$	$208 \times 208 \times 32$	$104 \times 104 \times 32$
4	Convolutional	64	$3 \times 3/1$	$104 \times 104 \times 32$	$104 \times 104 \times 64$
5	Maxpool		$2 \times 2/2$	$104 \times 104 \times 64$	$52 \times 52 \times 64$
6	Convolutional	128	$3 \times 3/1$	$52 \times 52 \times 64$	$52 \times 52 \times 128$
7	Maxpool		$2 \times 2/2$	$52 \times 52 \times 128$	$26 \times 26 \times 128$
8	Convolutional	256	$3 \times 3/1$	$26 \times 26 \times 128$	$26 \times 26 \times 256$
9	Maxpool		$2 \times 2/2$	$26 \times 26 \times 256$	$13 \times 13 \times 256$
10	Convolutional	512	$2 \times 2/2$	$13 \times 13 \times 256$	$13 \times 13 \times 512$
11	Maxpool		$2 \times 2/1$	$13 \times 13 \times 512$	$13 \times 13 \times 512$
12	Convolutional	1024	$3 \times 3/1$	$13 \times 13 \times 512$	$13 \times 13 \times 1024$
13	Convolutional	256	$1 \times 1/1$	$13 \times 13 \times 1024$	$13 \times 13 \times 256$
14	Convolutional	512	$3 \times 3/1$	$13 \times 13 \times 256$	$13 \times 13 \times 512$
15	Convolutional	255	$1 \times 1/1$	$13 \times 13 \times 512$	$13 \times 13 \times 255$
16	YOLO				
17	Route 13				
18	Convolutional	128	$1 \times 1/1$	$13 \times 13 \times 256$	$13 \times 13 \times 128$
19	Up-sampling		$2 \times 2/1$	$13 \times 13 \times 128$	$26 \times 26 \times 128$
20	Route 19 8				
21	Convolutional	256	$3 \times 3/1$	$13 \times 13 \times 384$	$13 \times 13 \times 256$
22	Convolutional	255	$1 \times 1/1$	$13 \times 13 \times 256$	$13 \times 13 \times 256$
23	YOLO				

2.2.2 Artificial neural networks

The structure of artificial neural networks has functional subunits called neurons or nodes. It is processor that receives input and computes an output shown in Figure 2.9. Each neuron associated with which weight factors ($w_1, w_2, w_3, \dots, w_n$) to determine the importance of input values ($x_1, x_2, x_3, \dots, x_n$). Each input signal is multiplied by the weight of the neuron connection, and there is bias that adjust the

output signal in discrete steps depending on the value of the summation of the input signals. Activation of the output neuron can be written in mathematical terms,

$$\text{Output of neuron} = \text{Activation function} \left(\sum_{i=1}^n x_i w_{ij} - \theta_j \right)$$

Where n is the number of input connections into unit j .

w_{ij} is the weight of the connection between unit i of the previous layer and unit j .

θ_j is the bias that adjusts the output signal to provide neuron with a trainable constant value.

Activation function is a function to convert the value obtained from the computation of the weight of the neural network structure.

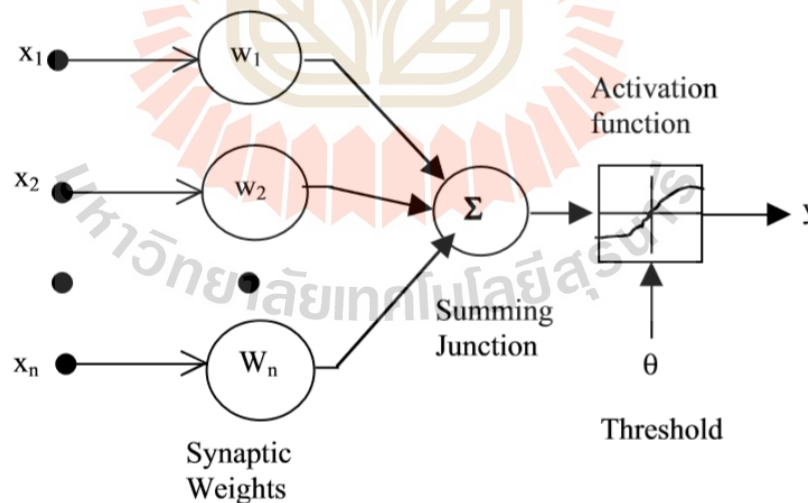


Figure 2.9 Basic elements of an artificial neuron (Jamshidi et al., 2001).

The activation functions are important mathematical operations to learn the complex patterns. Its role is to convert the activation of a neuron output y to an output. There are several activation functions that encounter as:

- Linear Function: returns the same value that was used as its argument.

$$f(x) = x, \quad -\infty \leq f(x) \leq \infty$$

- Sigmoidal function: returns the value input and squeeze the remaining values 0 to 1.

$$f(x) = \frac{1}{1 + e^{-x}}, \quad 0 \leq f(x) \leq 1$$

- Hyperbolic tangent function: resemble sigmoidal function. The difference is that the negative inputs will be mapped negative, and the zero inputs will be mapped near zero.

$$f(x) = \frac{e^x - e^{-x}}{e^x + e^{-x}}, \quad -1 \leq f(x) \leq 1$$

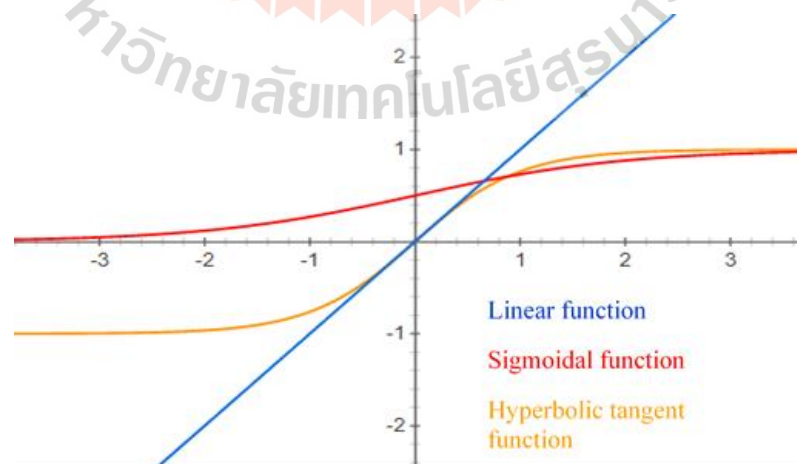


Figure 2.10 Comparison of the activation function.

In the previous, a single process of neuron has described. However, its effective implementation requires multiple neurons to perform more complex calculations. Multiple neurons arranged in a layer that can separated three types of layers:

- Input layer is a layer of neurons that receives input signals and transfers the signal to the network for processing. These may be either input signals or signals from other systems outside the simulated system.
- Hidden layers are layers of neurons that receive signals from the input layer and process them in a hidden manner. All connections from the hidden layer are to other layers within the system. When increasing processing power and efficient libraries, neural networks can be constructed. Complex learning can mean having many hidden layers in the neural networks.
- Output layer is a layer of neurons that receives processed signals and transfers output signals out of the system.

With controlling connections with neurons, the total number of layers, and the number of neurons in each layer determines the architecture of the neural network. There are two types of the architecture of artificial neural network such as single-layer perceptron and multi-layer perceptron. A single-layer perceptron consists of 2 layers as input layer and output layer, similar to a single of neuron as shown in Figure 2.11(a). It can only learn linear patterns and without any hidden layers. A multi-layer perceptron can accept various input formats and form complex decision regions in order to separate various nonlinear patterns. It consists of three or more

layers such as one input layer, one output layer and one or more hidden layers as shown in Figure 2.11(b).

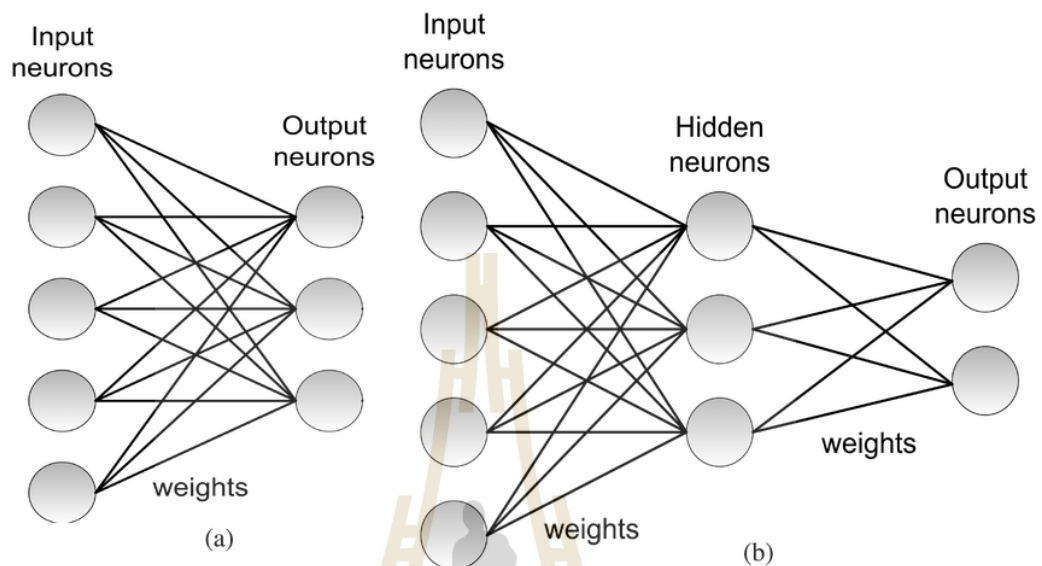


Figure 2.11 (a) Architecture of a single-layer perceptron, (b) Architecture of multi-layer perceptron (Camunas-Mesa et al., 2019).

2.3 Applied deep learning for electrospinning

2.3.1 Model application

The position of the droplet at the needle tip must be identified in order to identify the condition of stable and continuous production. However, the droplet at the tip is varied depending on electrospinning parameters. Therefore, the transformation of the droplet shape must be constantly inspected. The Taylor cone and bottom curve droplet positions are tracked using the object detection model. This model is expected to study the condition of electrospinning parameters that needed to maintain the droplet shape. Additionally, a classification model is used to consider the droplet

shape while analyzing the influence of droplet shape on fiber production. Finally, the efficient of the object detection and classification models is evaluated.

2.3.2 Evaluation classification model

The efficient of classification model is mainly measured in the confusion matrix as shown in Table 2.4. It represents counts from predicted and actual values on each class (Kulkarni et al., 2020). It is an important table and helpful for measuring the efficient of classification model.

Table 2.4 Confusion matrix.

Case NO.	Actual value	Model predicted	Result
1	Yes	Yes	True Positives (TP)
2	Yes	No	False Negatives (FN)
3	No	Yes	False Positives (FP)
4	No	No	True Negatives (TN)

Where True Positives (TP): Predicted as correctly on event values.

True Negatives (TN): Predicted as correctly on no-event values.

False Positives (FP): Predicted as incorrectly on event values.

False Negatives (FN): Predicted as incorrectly on no-event values.

Confusion matrix is used to calculate accuracy, precision, recall and F_1 score.

They are widely used for classification. Accuracy is the most commonly for evaluating performance, which is a measure of the accuracy of the model by considering all classes. Precision represents accuracy of the model that predicts positive values. Recall represents how accurate the model for correctly predicting

positive classes (Kulkarni et al., 2020). And F_1 score is a value that calculate from weighted harmonic mean between the precision and the recall (Fernández et al., 2018). The four methods of calculation can be written as following:

- Accuracy is the proportion of correct predictions.

$$\text{Accuracy} = \frac{\Sigma \text{True Positive} + \Sigma \text{True negative}}{\Sigma \text{Total population}}$$

- Precision measures how accurate the predictions are.

$$\text{Precision} = \frac{\Sigma \text{True Positive}}{\Sigma \text{Predicted condition positive}}$$

- Recall measures how well that find all the positives.

$$\text{Recall} = \frac{\Sigma \text{True Positive}}{\Sigma \text{Condition positive}}$$

- F_1 score is the harmonic mean of the precision and recall.

$$F_1 \text{ score} = \frac{2 \cdot \text{Precision} \cdot \text{Recall}}{\text{Precision} + \text{Recall}}$$

CHAPTER III

METHODOLOGY

This chapter outlines the experimental procedure, which is divided into two sections. The first section involves the setup of the electrospinning apparatus, preparation of the polymer solution, and defining the boundaries of the experiment for collecting dataset. The second section details the process of acquiring and training the datasets. In addition, some challenges encountered during the compilation of the dataset will also be discussed. Finally, the effectiveness of the model is then evaluated using a confusion matrix.

3.1 Electrospinning set-up

Conventional electrospinning system was used in this research. It is a typical vertical set-up for all the experiments. The electrospinning process was performed at 25 ± 2 °C and relative humidity at 48-52%. Polyethylene oxide (PEO, Mw = 600,000 g/mol) was purchased from Sigma-Aldrich, USA. The PEO aqueous solutions were prepared by dissolving 2, 4, 6 w/w% of the sample in distilled water separately via a magnetic stirrer (IKA® C-MAG HS hotplate stirrers) at 70 °C for 48 hours. The solution was loaded into a 10 mL syringe. A syringe pump (Terumo - Terufusion TE-311 syringe pump) was used to control the flow rate of the PEO solution through a Polyvinyl Chloride (P.V.C.) tube. The P.V.C. tube was connected at one end with the

syringe and the other end with a blunt needle tip (18G, O.D. = 1.27 mm, and I.D. = 0.84 mm). A high-voltage power supply (YKY, 50 kV power supply for electrospinning system) was attached to the needle to apply an electric potential. The collector is a flat 20 cm x 20 cm aluminum foil plate located under the needle. The electrospinning set-up is shown in Figure 3.1. Following the experiment, the morphologies of the fibers were examined using a scanning electron microscope (JEOL Model JSM-6010LV). The SEM images revealed the formable nature of fiber products that can be controlled with the electrospinning parameters.

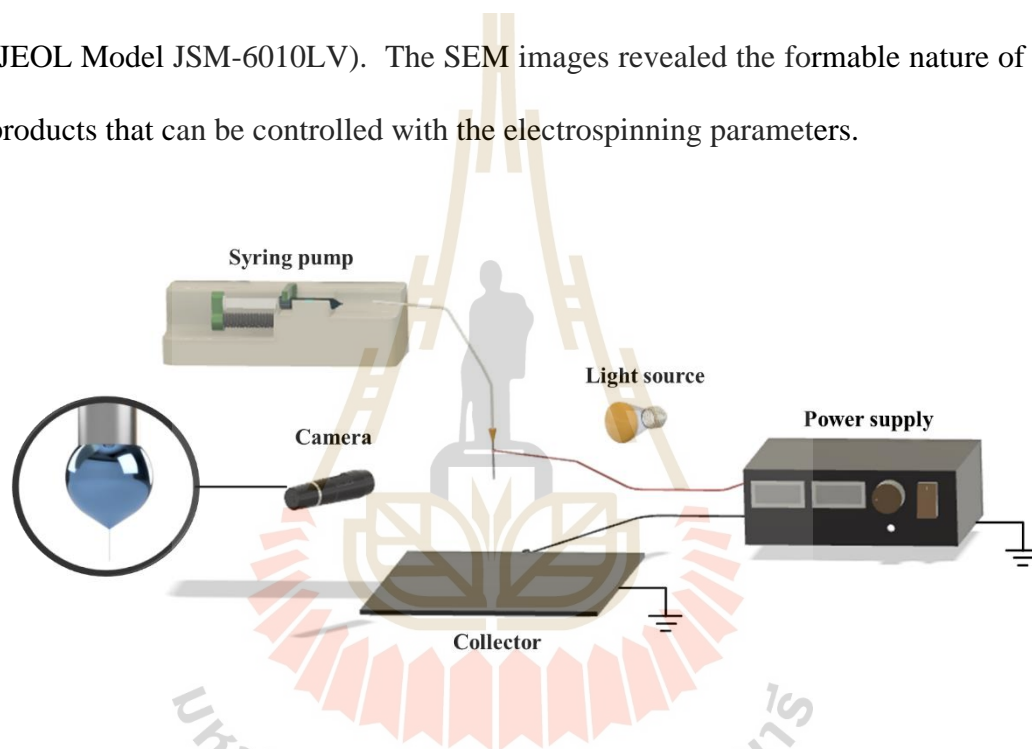


Figure 3.1 Schematic diagram of electrospinning set-up.

The influence parameters that affect the electrospinning manufacturing process were varied and observed. The tip-to-collector distance (TCD), flow rate, and applied voltage were controlled. The TCD was set up at 5, 10, and 15 centimeters, and the flow rate was set up at 1, 2, 3, and 4 ml/h. In each case, the applied voltage was continuously increased from 0 to 15 kV at a rate of 2 kV/min.

3.2 Dataset obtaining and model training

3.2.1 Object detection model

The study of the effect of the Taylor cone on fiber production required some production data, and then the correlation pattern could be obtained. A camera (IMSHI 1600X Digital Microscope USB Endoscope Camera) was placed in front of the needle to record the droplet at the tip of the needle with a backlit light source in the background. In each video, a droplet at the tip of the needle was recorded in the electrospinning process. But in this section, when using a high voltage, the problem encountered was that it created a strong electric field, causing the camera to malfunction. As a result, the datasets did not contain all the data as intended. To solve this problem, the video was only recorded at the range where the electric field had no effect on the camera. Four datasets were created by repeating the experiment four times for each condition. A dataset was selected as a training dataset, and the rest were validated datasets.

The videos from the dataset were extracted to capture frame images by capturing every second. Cira core software was used in this work to label the information position and model training. The deep training tool in the Cira core was used in the section on target labeling to label the location of the Taylor cone and bottom curve droplet in the image by collecting 512 images for the training images. Figure 3.2 shows the process of labeling the image.

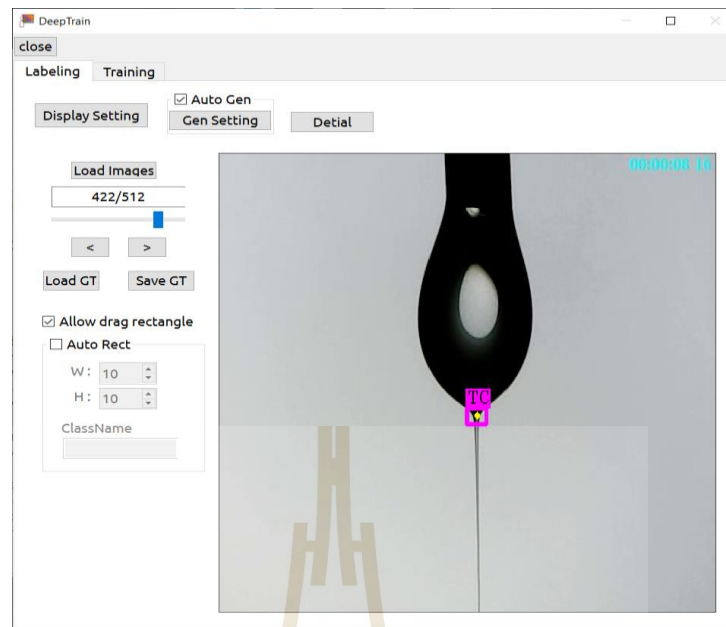


Figure 3.2 Labeling the target and contains position of the target.

However, there are similar background environments for the 512 training images. It may cause the prediction of the model to be inaccurate due to external disturbances such as uneven image brightness. They are solved with data enhancement by increasing some training data. Enhancement methods were used to generate the images to extend the dataset. The images were rotated 90°, 180°, and 270°, and the contrast was adjusted in 0.1-step increments from 0.4 to 1.1. Figure 3.3 shows an example of image enhancements. YOLOv3 tiny model in the Cira core, which is a deep convolutional network structure for object detection, is used to store the location of the Taylor cone of images. After training the model, the results from the training were evaluated on a validated dataset of 102 images.

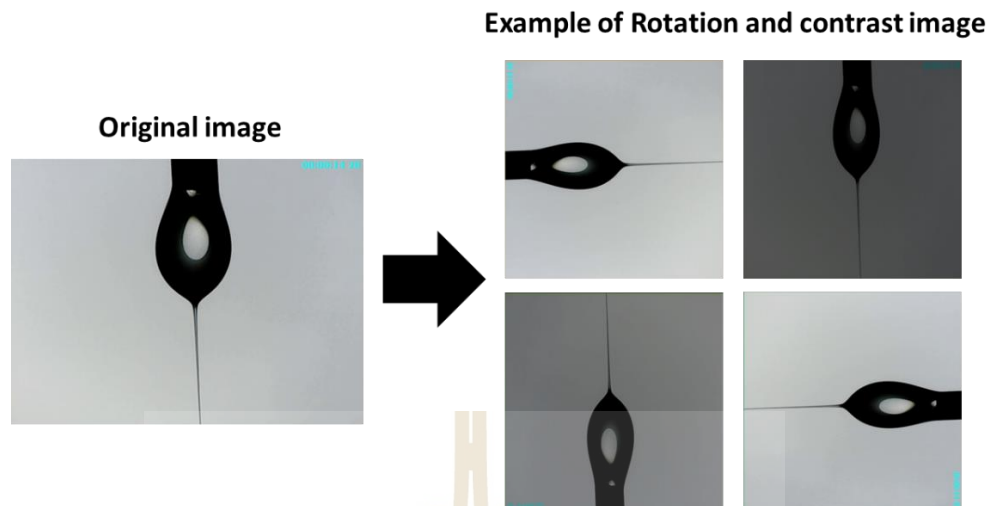


Figure 3.3 Dataset enhancements.

The next process is evaluating a model, which is as important as building one. Because a model must perform with previously unknown data, a thorough and varied evaluation is required to build a robust model. The confusion matrix intersection over union (IoU) was selected to evaluate the model section. IoU is a term used to describe the overlap between the predicted bounding box and the truth bounding box in each image, as shown below:

$$\text{Intersection over union (IoU)} = \frac{\text{Area of Overlap}}{\text{Area of Union}}$$

The IoU threshold was used for deciding whether an IoU was a True Positive (TP) or False Positive (FP). A false negative (FN) is the failure to predict an actual target. In this work, an IoU threshold value of 0.5 was used. Precision and recall, which measure accuracy in prediction models, can be calculated to determine whether the model was suitable for predictions or not using the following equations:

$$\text{Precision} = \frac{TP}{TP + FP}$$

$$\text{Recall} = \frac{TP}{TP + FN}$$

In addition, the important evaluation indicates the efficiency of the model, and the F1 score can be calculated as follows:

$$F_1 \text{ score} = \frac{2 \cdot \text{Precision} \cdot \text{Recall}}{\text{Precision} + \text{Recall}}$$

Therefore, the implementation part that can be written as a flow chart for the training model is shown in Figure 3.4.

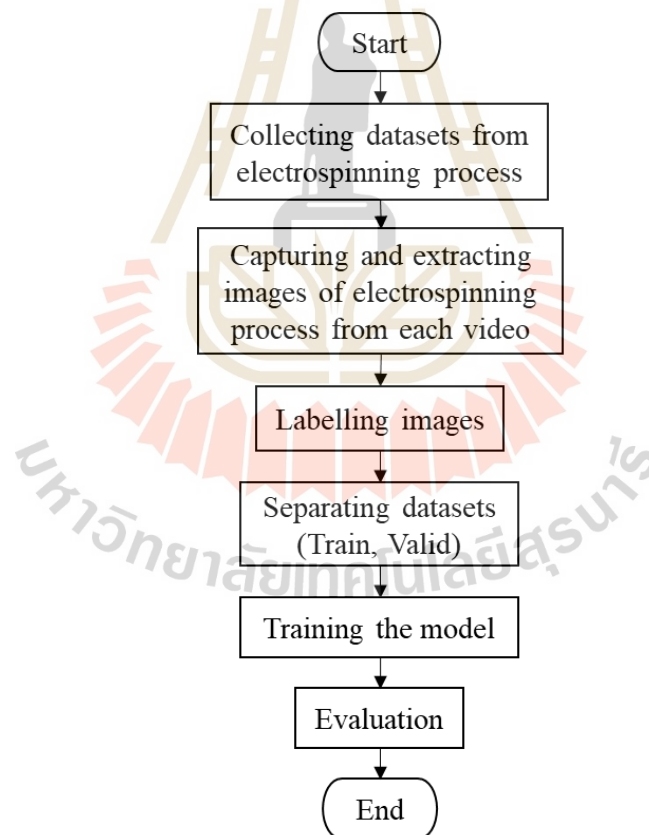


Figure 3.4 Flow chart for training model.

3.2.2 Classification model

The dataset for the classification was the shape of the Taylor cone, as shown in Figure 3.5. The datasets were obtained by capturing the experiment videos of all conditions and partially randomizing the datasets. After that, they were categorized into 664 images consisting of 4 classes such as dripping, droplet-jet, cone-jet, and rotational, with the numbers of images being 200, 200, 200, and 64, respectively. Enhancement methods were used to generate the new images. The images were rotated by 90° , 180° , and 270° , and contrast was adjusted at 0.4-1.1 by 0.1 steps using the same detection enhancement model. A deep training tool in the Cira core was used for training the Taylor cone. After training the model, the validated dataset of 166 images was used to evaluate the model.

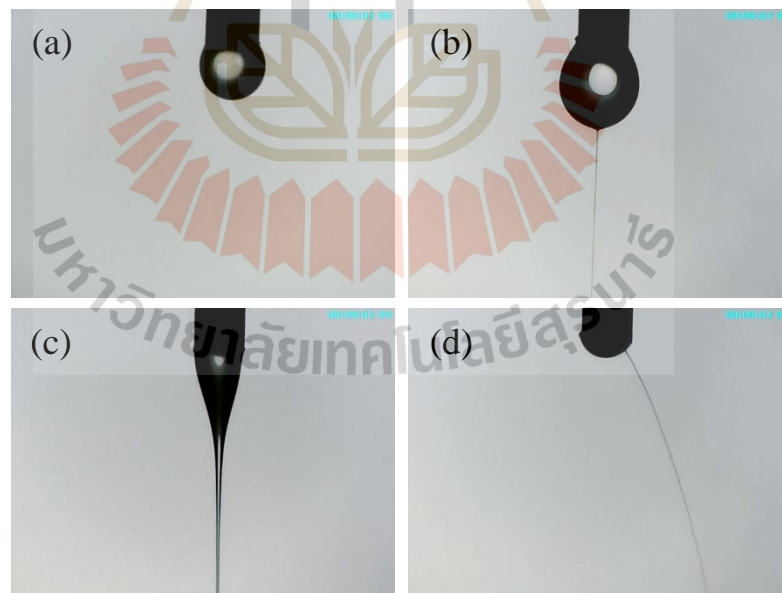


Figure 3.5 Example of image data from the training datasets: (a) dripping, (b) droplet-jet, (c) cone-jet, (d) rotational.

CHAPTER IV

RESULTS AND DISCUSSION

The model performance and discussion results are presented in this chapter. The confusion matrix is used to evaluate effectiveness of the model. The model is then used to analyze experiment videos to identify correlations among the electrospinning parameters. The following results of this work can be described as the following:

- Result I: Model performance
- Result II: Correlations between flow rate and voltage
- Result III: The boundary map of fabricated fibers
- Result IV: Identification of regimes
- Result V: Additional experiments and study comparisons

4.1 Result I: Model performance

4.1.1 Object detection model

An evaluation is needed to determine the effectiveness of the implementation methodology for tracking a jet's transition. In all 512 photos (representing 80% of all images), the location of the Taylor cone and the lowest curve droplet were used as the training image. In the evaluation, 122 photos (representing 20% of all images) from

the validation dataset was used. The predicted positions of the validation dataset were plotted in comparison to the truth positions. Since the droplet expansion on the y-axis is already known, it is simply considered. The projected location on the y-axis of the Taylor cone and the truth position on the y-axis can be shown on a graph, as seen in Figure 4.1.

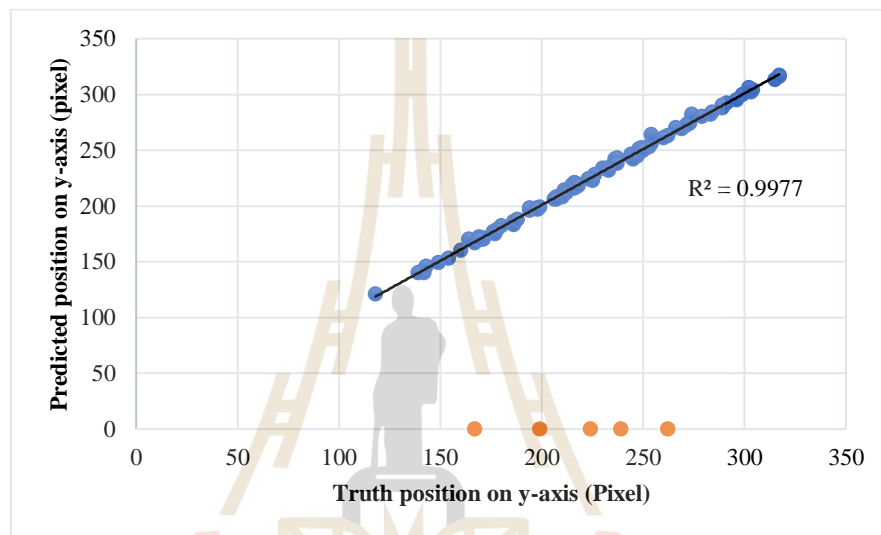


Figure 4.1 Comparison between truth and prediction position.

R-squared (R^2) was chosen as a consideration since Figure 4.1 is a model of linear regression. The y-axis of Taylor cone has a predicted position on it that is 99.77% congruent with the truth position on it, according to the R-squared of axis y. Additionally, 5 data points (orange dots) from the validation dataset failed to identify the Taylor cone, resulting in an overall model effectiveness of 95.9%. This indicates that the object detection model has a high level of performance.

4.1.2 Classification model

This study implemented a classification model for categorizing the Taylor cone shape. The training dataset contains 664 images, divided into four regimes: dripping, droplet-jet, cone-jet, and rotational, with 200, 200, 200, and 64 images, respectively (representing 80% of the total images). In the validation section, a total of 166 images were used, divided into 50, 50, 50, and 16, respectively (representing 20% of the total images).

Table 4.1 provides a summary of the results obtained from the confusion matrix. In this study, 166 images were evaluated, and 150 of them were properly predicted, resulting in overall accuracy of 90.4%. The model has the highest precision, recall and F1 score, of 100% in the droplet class. For droplet-jet and cone-jet classes, there are incorrect predictions in a small number of images. This is because there was a cross-class prediction because the class transitions were similar. The model showed slightly less accurate predictions in the rotational class due to a smaller number of datasets compared to the other classes. The average accuracy of the results is 87.2% with a target detection accuracy of 92.0%, and F1 score of 87.1%.

Table 4.1 Summarize the results obtained from the confusion matrix.

Class	Accuracy (%)	Precision (%)	Recall (%)	F1 score (%)
Dripping		100.0	100.0	100.0
Droplet-jet	90.4	100.0	98.0	99.0
Cone-jet		97.2	70.0	81.4
Rotational		51.6	100.0	68.1
Average		87.2	92.0	87.1

4.2 Result II: Correlations between flow rate and voltage

The experiment involved videos capturing frame images every second. As seen in Figure 4.2, these images were tracked with the Taylor cone using the object detection model to examine the deformation of droplet. To facilitate understanding, only the y-axis of the Taylor cone was considered. The position at the top of the boundary image was defined as 0 and increased as the position moved downward within the image.

**Figure 4.2** Example of Taylor cone detection.

Some issues were discovered and encountered during the experiment. Some of the frame images were unable to be tracked the Taylor cone. As seen in the graph in Figure 4.3(a), these positions were assigned a value of 0. To overcome this challenge, the position values surrounding the problematic positions were averaged. This improvement is reflected in the graph of the Taylor cone's tracking along the y-axis and time as shown in Figure 4.3(b).

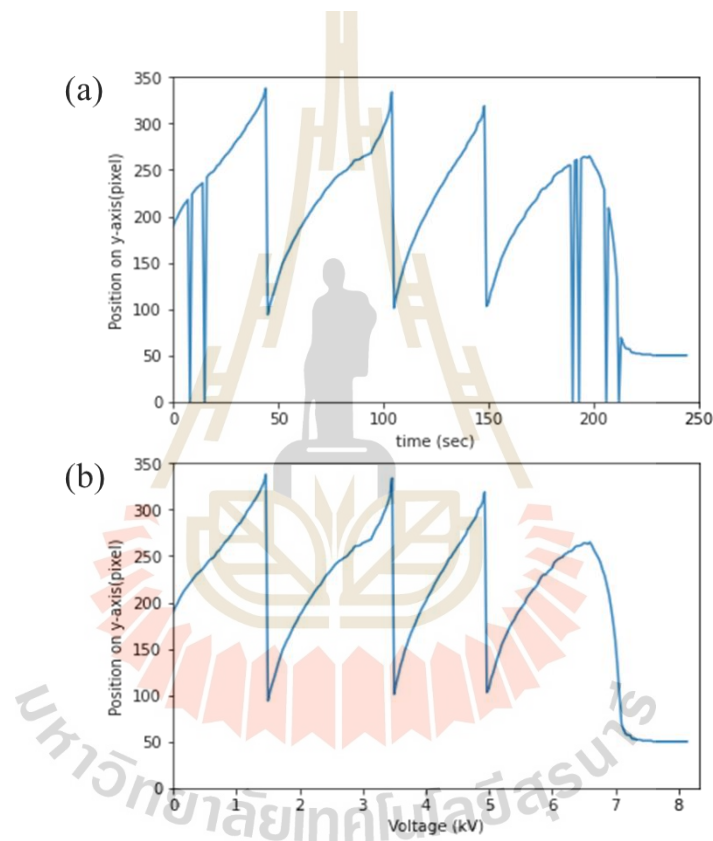


Figure 4.3 (a) the example graph of tracking Taylor cone on y-axis and time. (b) the example graph of tracking Taylor cone on y-axis and voltage after improvement.

As depicted in Figure 4.3(b), the first three peaks are characterized by sharp spikes, while the last peak has a smooth curve. For the analysis, firstly, considering only the first three sharp peaks during the period of increasing y-axis values. This signifies that the droplet at the tip of the needle expands, until the y-axis position starts to decline rapidly. The decline is due to gravity, causing the droplets to fall from the tip of the needle. These sharp peaks indicate that the flow-in rate is higher than the flow-out rate.

Secondary, considering the last smooth peak, the final peak has three components to consider. The ascending slope represents expansion of the droplet or that the flow-in rate is greater than the flow-out rate. Conversely, the descending slope signifies shrinking of the droplet or that the flow-in rate is lower than the flow-out rate. It can be argued that the apex of the final peak represents a balance between the flow-in rate and the flow-out rate, which maintains a stable Taylor cone and continuous fiber production. This stability is key to controlling the shape of the Taylor cone.

To determine the time or voltage value at the final peak, a polynomial equation of degree six is generated. The voltage at which the flow-in and flow-out rates are equal is calculated by solving the polynomial equation. The results for the r-squared of the polynomial and the x-axis position of the peak as a function of time and voltage are presented in Figure 4.4.

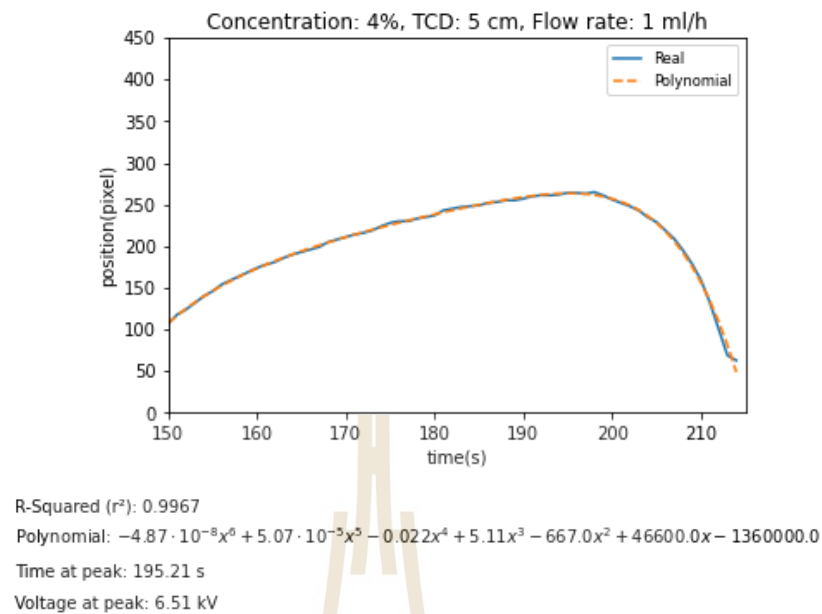


Figure 4.4 The example of analysis results at the last peak.

To further examine the relationship between voltage and flow rate, the concentration of polymer solution was separated into three separate graphs, with each data point representing an average of three validated datasets that represent a balance between the flow-in rate and the flow-out rate.

The results, displayed in Figure 4.5, indicate a direct proportional relationship between flow rate and voltage in Figure 4.5(a) and (b). It is notable that when comparing the same flow rate and TCD, higher concentrations of 4%wt result in higher voltages compared to 2%wt concentrations. As the flow rate increases, the voltage required to initiate the electrospinning process also tends to increase. This is because a higher flow rate requires a higher electrostatic force to overcome the surface tension and viscosity of the solution and to form a stable jet (Huang et al., 2004; Iregui et al., 2019).

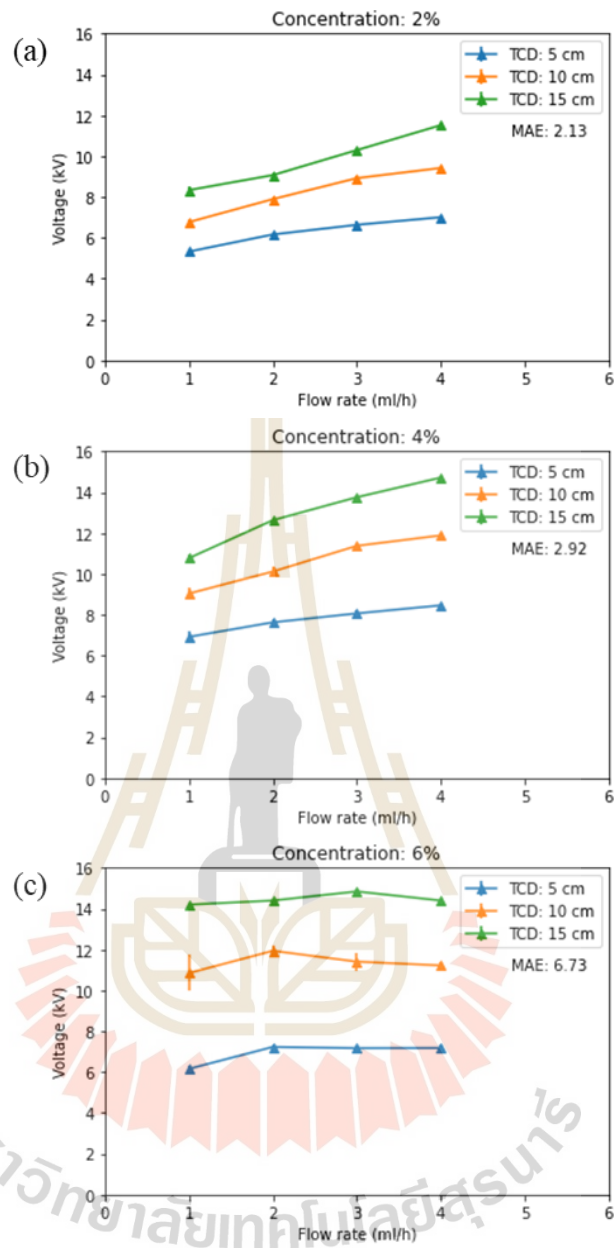


Figure 4.5 Correlations between flow rate and voltage for the stable Taylor cone shapes at concentration (a) 2% wt, (b) 4% wt, and (c) 6% wt.

However, it contradicts the concentration of 6%wt results that were previously observed, which showed the voltage changes slightly with increasing flow rate as shown in Figure 4.5(c). Because there is an upper limit to the concentration beyond which the electrospinning process becomes unstable, and the required voltage may increase or decrease depending on the specific properties of the polymer solution. At excessively high concentrations, the charge density on the surface of the droplet can become too high, leading to instability and the formation of beads or droplets instead of fibers (Xue et al., 2019; Zaitoon et al., 2020).

4.3 Result III: The boundary map of fabricated fibers

To determine the optimal electrospinning parameters, fibers were collected during the experiment under varying conditions, including concentration levels of 2%, 4%, and 6%wt, TCD values of 5, 10, and 15 cm, flow rates of 1, 2, 3, and 4 ml/h, and voltages ranging from 0 to 15 kV in increments of 1 kV. The morphologies of the fiber products were examined using scanning electron microscopy (SEM).

The objective was to determine the conditions under which fibers could be produced and identify any areas on the collector that did not produce fibers. This information was used to distinguish between fiber and non-fiber samples (details can be found in Appendix A).

The morphologies of the collected fibers were analyzed based on the conditions under which they were produced. It was found that when the flow-in rate was greater than the flow-out rate, the flow rate had no significant effect on the

fabricated fibers. This was observed even when the flow rate was changed, as the results remained the same (the droplet solution did not fall off the collector).

The correlation between voltage and TCD can be plotted on a graph as shown in Figure 4.6. It can be seen from Figure 4.6(a) that a concentration of 2%wt does not result in pure fibers, but rather a mixture of fibers and beads (details in Appendix A). This is because low concentration solutions lead to electro spray rather than electrospinning (Huang et al., 2003; Karakaş, 2015). Figure 4.6(b) and (c) show that concentrations of 4%wt and 6%wt can produce fibers, with 6%wt having a wider range of fabrication than 4%wt. As the lower concentrations of the polymer solution generally result in smaller fiber diameters, and higher surface area, but can also lead to decreased fiber uniformity and instability in the electrospinning process. On the other hand, the concentration of the polymer solution is increased, the viscosity of the solution also increases, which affects the stretching of the jet and the resulting fiber diameter. Specifically, as the concentration is increased, the fiber diameter generally increases due to the higher viscosity of the solution that resists stretching of the jet. Additionally, the surface tension of the solution also increases with concentration, which can result in the formation of beads or droplets rather than fibers if the electrostatic force is not sufficient to overcome the surface tension (Huang et al., 2003; Li and Xia, 2003).

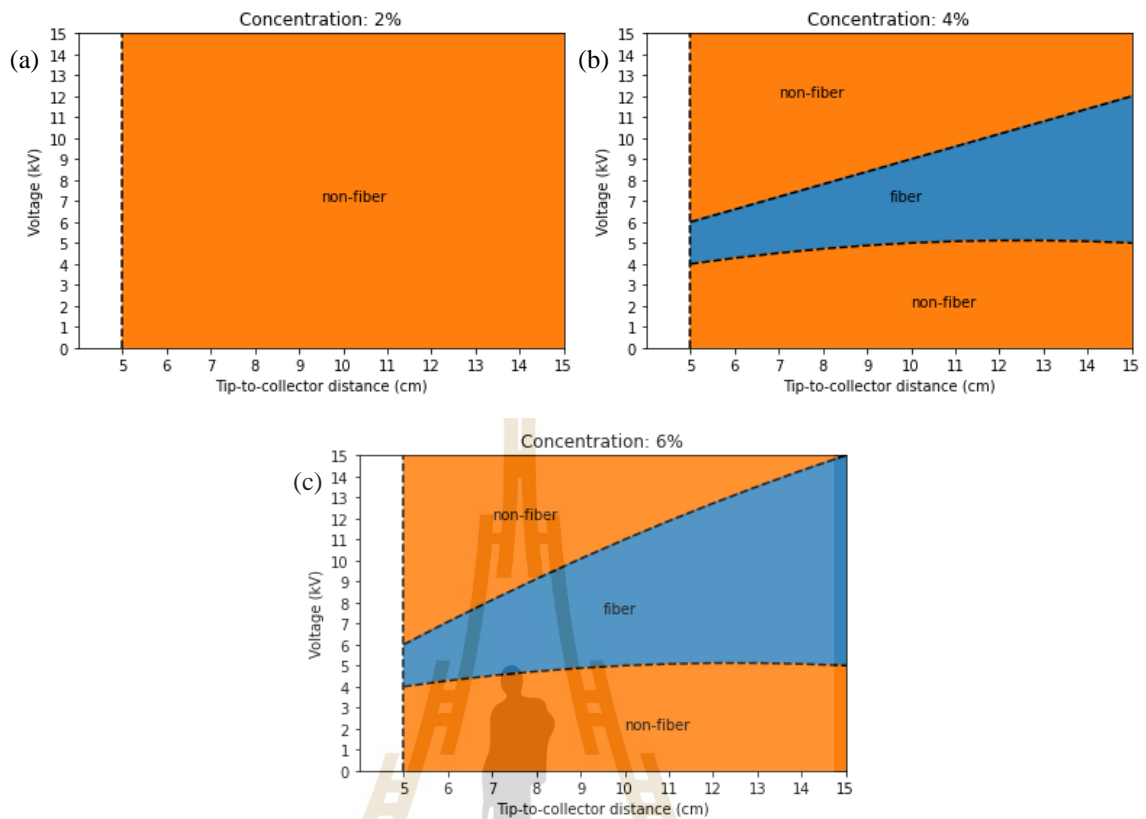


Figure 4.6 The boundary map of fabricated fibers at concentration (a) 2% wt, (b) 4 % wt, and (c) 6% wt.

4.4 Result IV: Identification of regimes

A classification model was used to categorize the shape of the droplet at the tip of the needle while controlling the relationship between TCD and voltage at different flow rates. The results can be classified into four regimes: dripping, droplet-jet, cone-jet, and rotational. They can be plotted at voltage and TCD rate for concentration and flow rate variations, as shown in Figures 4.7-4.9. The brief details of the regimes are given below.

The dripping regime is the boundary at which the electric field has not yet reached a critical value (V_c), so that the surface of the droplet was not elongated into the fibers. When the polymer solution flows into the droplet at the tip of the needle to increase droplet size, the droplet is caused to drip by gravity force greater than the adhesive force between the polymer droplet and the tip of the needle.

The droplet-jet regime is a boundary where the electric field attains a critical value and affects the shape of the droplet. The surface of the droplet is elongated by the jet to reach the collector. The results show that there is uncertainty for entering the droplet-jet regime because the dripping of solution has a great effect on the initial entry into the droplet-jet regime. The droplet-jet regime starts with the emergence and transformation of a jet and continues until the flow-in rate equals the flow-out rate.

The cone-jet regime is a regime that starts with the flow-in rate being less than or equal to the flow-out rate. This regime is formed in a conical shape, and it can continually fabricate as there is no dripping. However, it would cause the Taylor cone to shrink into the needle and interrupt production if the flow-in rate is much less than the flow-out rate. Also, this regime is not found at low concentrations because the surface tensions of the solution is less than the electric force. This makes it unable to stabilize itself and fall out of the tip of the needle.

Lastly, **the rotational regime** is similar to the cone-jet regime, but with an increased voltage, the transformation of a jet becomes rotational at the central axis of the needle. If the voltage continues to increase, the flow-in rate becomes much less

than the flow-out rate, causing the transformation of the jet to shrink into the needle and breaking fiber production during fabrication.

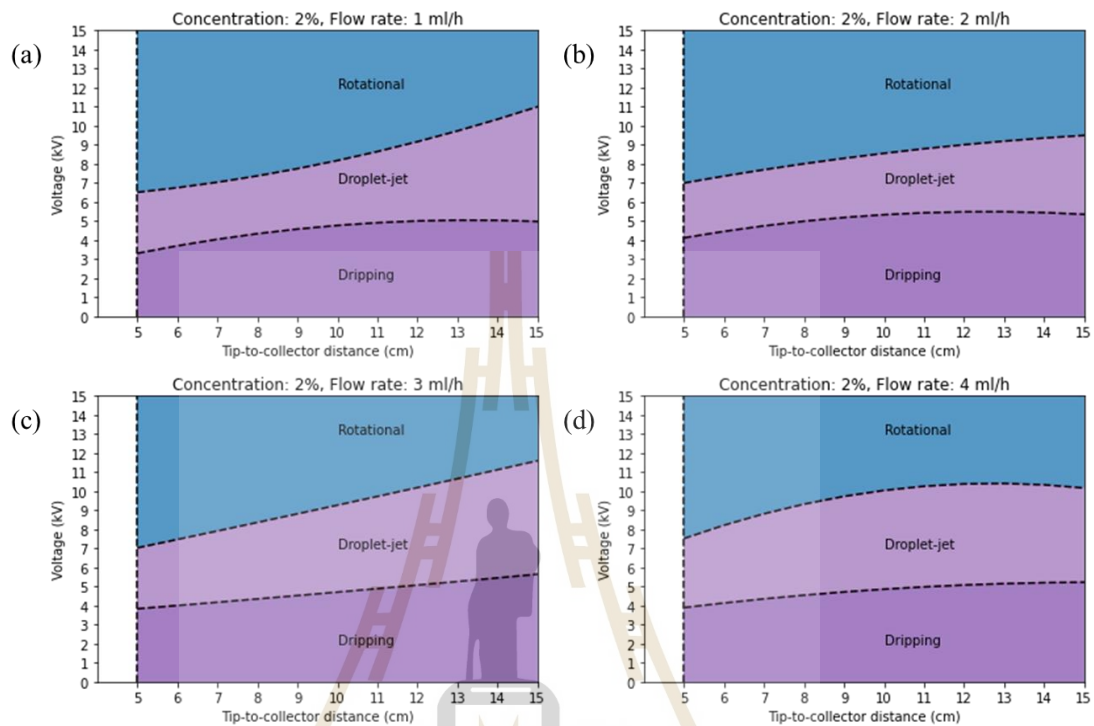


Figure 4.7 Regime map generated of concentration: 2% wt by controlling tip-to-collector distance and voltage at flow rate (a) 1 mL/h, (b) 2 mL/h, (c) 3 mL/h, (d) 4 mL/h.

At a concentration of 2% wt, the results can be classified into three regimes: dripping, droplet-jet, and rotational, as shown in Figure 4.7. The cone-jet regime is absent because the surface tensions of the solution are less than the electric force. This results in no deformation of droplets and falls out to the ground. The unpredictability of the droplet-jet regime is notable, one factor that can contribute to the emergence of the droplet-jet regime is an increase in the flow rate of the polymer solution. As the flow rate is increased, the electrostatic force on the polymer solution can become

insufficient to maintain a stable jet, leading to the formation of droplets. Another factor that can affect the formation of droplets is the distance between the spinneret and the collector. When the distance is too short, the polymer jet may not have enough time to stabilize, leading to the formation of droplets (Darrell et al., 1996; Li, Wang, et al., 2003).

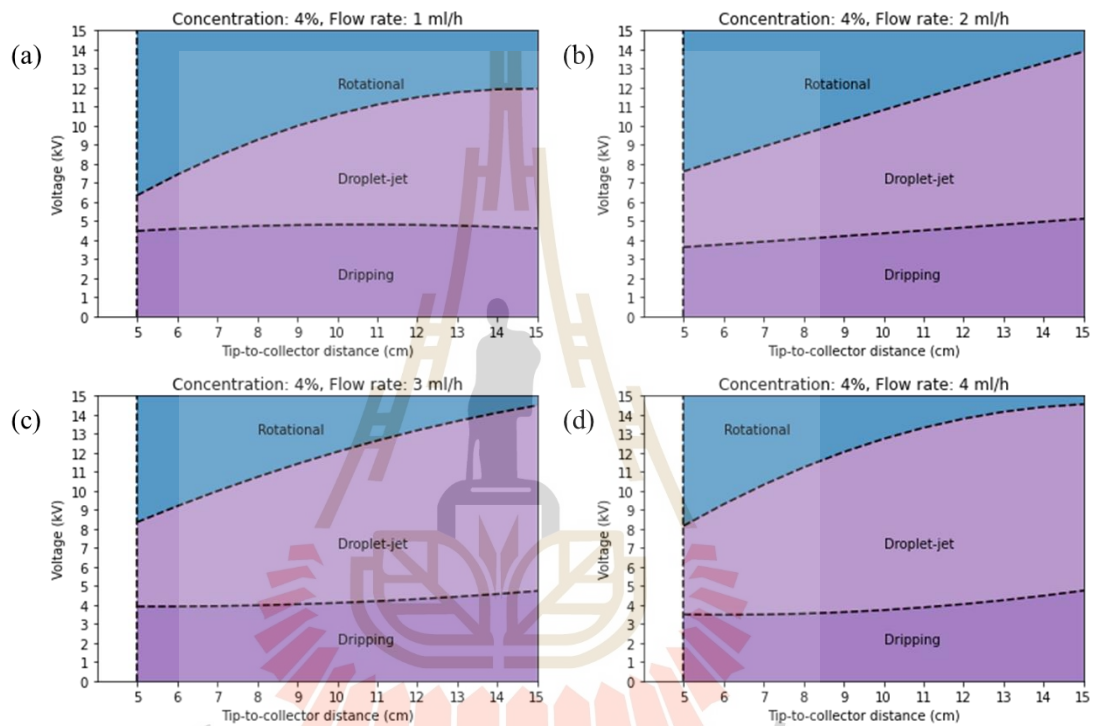


Figure 4.8 Regime map generated of concentration: 4%wt by controlling tip-to-collector distance and voltage at flow rate (a) 1 mL/h, (b) 2 mL/h, (c) 3 mL/h, (d) 4 mL/h.

As demonstrated in Figure 4.8, the results at a 4%wt are similar to the 2%wt concentrations and categorized into three regimes: dripping, droplet-jet, and rotational. In comparison to the results at 2%wt, the droplet-jet regime has a wider range, while the rotational regime has a smaller range. This is due to the increase in

concentration, which leads to a higher viscosity, yet still insufficient to cause droplet deformation and fall to the ground.

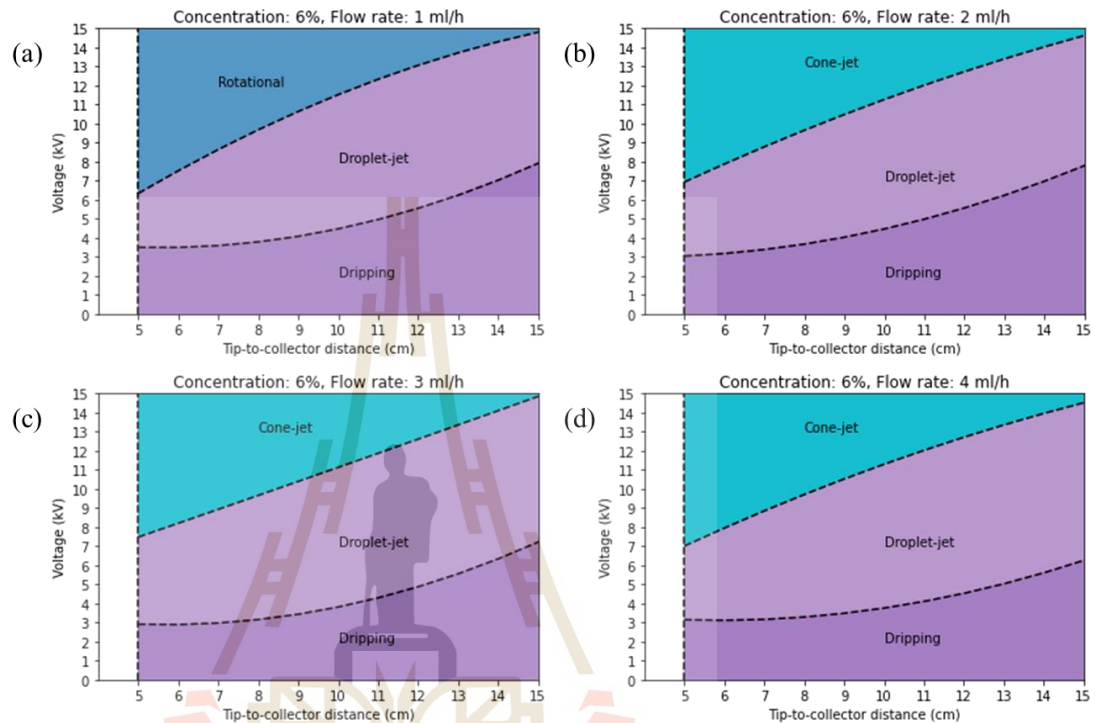


Figure 4.9 Regime map generated of concentration: 6%wt by controlling tip- to-collector distance and voltage at flow rate (a) 1 mL/h, (b) 2 mL/h, (c) 3 mL/h, (d) 4 mL/h.

At a concentration of 6%wt, the results can be classified into four regimes: dripping, droplet-jet, cone-jet, and rotational, as shown in Figure 4.9. However, there is no cone-jet regime present at a flow rate of 1 mL/h, as depicted in Figure 4.9(a). This is due to the electric force being insufficient to deform the droplet, and the flow-rate being lower than the flow-out rate, causing the Taylor cone to shrink into the needle and resulting in a rotational regime. Conversely, there is no rotational regime

observed at flow rates of 2, 3, and 4 mL/h, as seen in Figures 4.9(b), (c), and (d). This is because the voltage range studied was not high enough to significantly reduce the flow-in rate relative to the flow-out rate. In addition, high concentrations of the polymer solution result in increased viscosity, which can make it difficult to control the rheology, and the transition regime does not show a clear trend, which is consistent with the findings of Sukigara and coworkers (Sukigara et al., 2003).

4.5 Result V: Additional experiments and study comparisons

4.5.1 Continuous fabrication

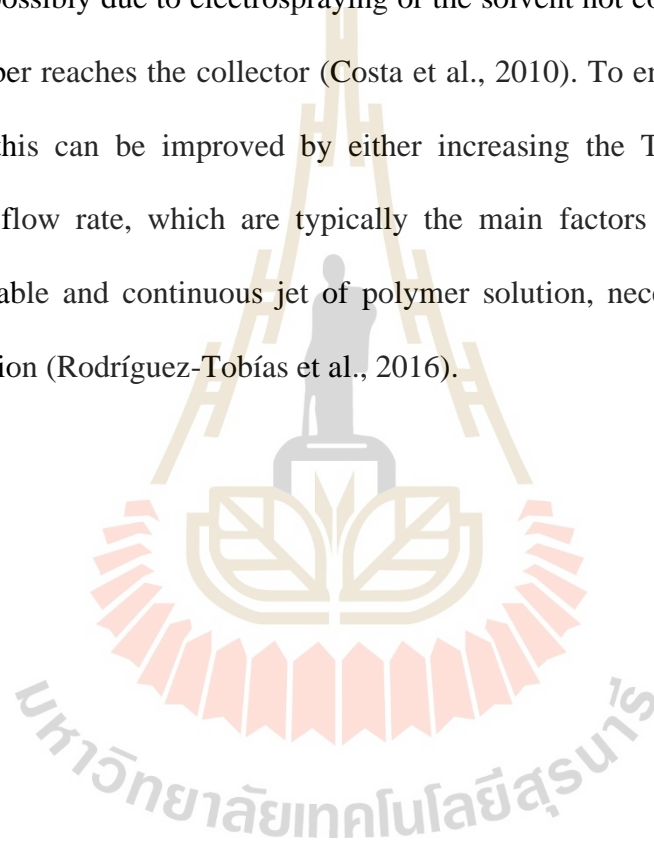
The correlation between flow rate and voltage for stable Taylor cone shapes, as well as the boundary map of fabricated fibers, are presented in Figure 4.10. This map was created to identify the conditions necessary for continuous fiber production.

It can be observed from Figure 4.10(a) that it is not possible to fabricate pure fibers at a concentration of 2% wt due to the low concentration of the solution. Similar to the study conducted by Deitzel and coworkers, it has been observed that electrospay occurs instead of electrospinning at very low concentrations (Deitzel et al., 2001). Figures 4.10(b) and (c), on the other hand, indicate that certain voltage and flow rate conditions were identified that enable the fabrication of continuous fibers, revealing a trend towards favorable electrospinning parameters for producing continuous fibers.

Additionally, it is apparent from Figure 4.10 that the area under the flow rate curve, representing the flow-in rate, is greater than the flow-out rate due to issues with

fiber production such as dripping onto the collector. The area above the flow rate curve, representing the flow-in rate, is less than the flow-out rate, which is caused by the shrinkage of the droplet into the needle, leading to discontinuous fiber production or fiber breakage during fabrication.

A period of equal flow-in and flow-out rates may result in non-fiber production, possibly due to electrospaying or the solvent not completely evaporating before the fiber reaches the collector (Costa et al., 2010). To ensure continuous fiber production, this can be improved by either increasing the TCD or adjusting the voltage and flow rate, which are typically the main factors that are modified to produce a stable and continuous jet of polymer solution, necessary for continuous fiber production (Rodríguez-Tobías et al., 2016).



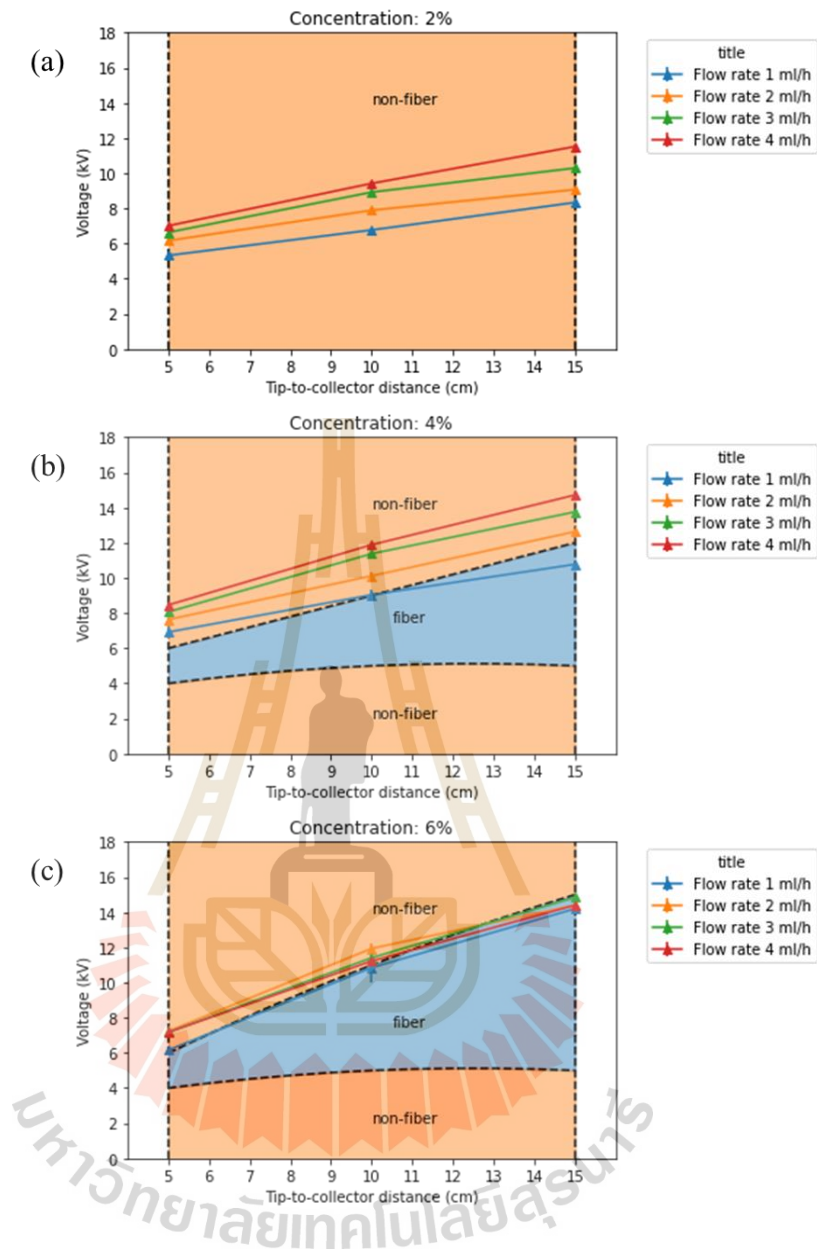


Figure 4.10 The boundary map of fabricated fibers with curve of flow-in rate equal flow-out rate at concentration (a) 2% wt, (b) 4% wt, (c) 6% wt

4.5.2 Continuous production on regime map

Knowing the type of regime that can fabricate continuous fibers is essential for controlling Taylor cone shape. A regime map can be plotted by combining the curve of flow-in rate equal to flow-out rate, as shown in Figures 4.11-4.13. From the graph, the following information can be found.

At concentration 2%wt and 4%wt was found that fabricating continuously is in the droplet-jet regime. However, Figures 4.11(d), 4.12(a), and 4.12(d) have some curves of flow-in rate-equal-flow-out rate fibers in the rotational regime. That is why the syringe pump was discontinued in some experiments. As a result, there is a lack in the flow of the solution, resulting in a faster entry into the next regime.

At a concentration of 6%wt, continuous fabrication can occur in either the droplet-jet and cone-jet regimes, depending on the flow rate. At a flow rate of 1 mL/h, only a droplet-jet regime is present because the electric force is not strong enough to deform the droplet. At flow rates of 2, 3, and 4 mL/h, the type of regime is determined by the volume of the droplet at the needle tip. If the droplet has a small volume, it will deform into the cone-jet regime. In addition, if the volume is large, the droplet-jet regime remains unchanged.

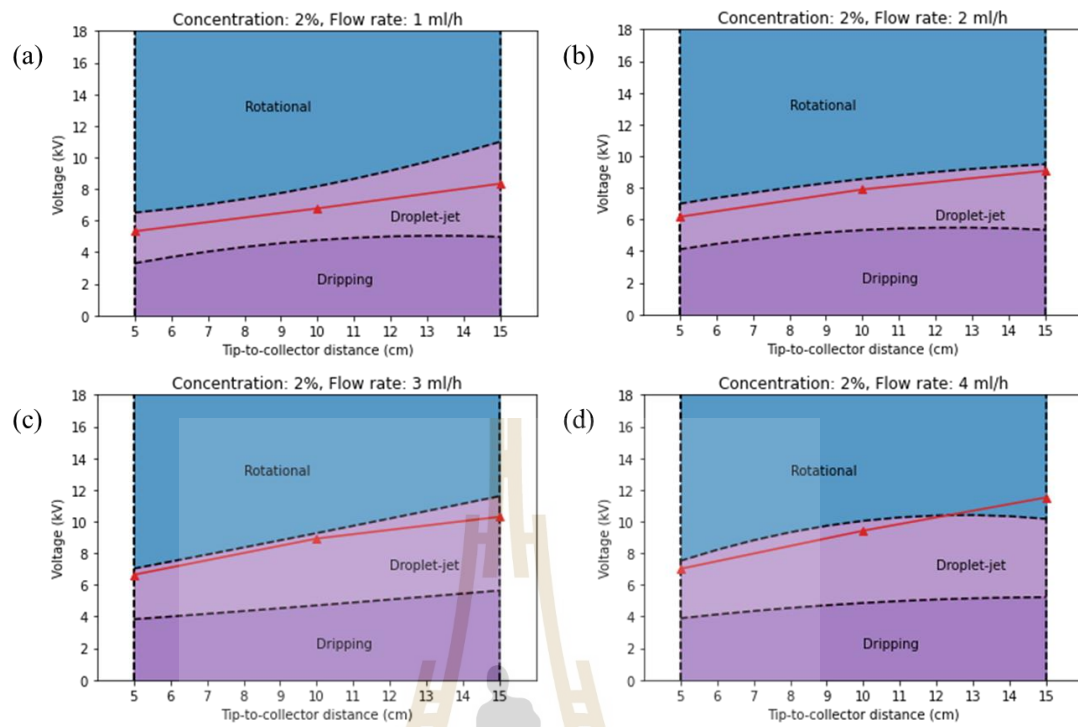


Figure 4.11 Regime map generated of concentration: 2% wt with curve of flow-in rate equal flow-out rate by controlling tip-to-collector distance and voltage at flow rate (a) 1 mL/h, (b) 2 mL/h, (c) 3 mL/h, (d) 4 mL/h.

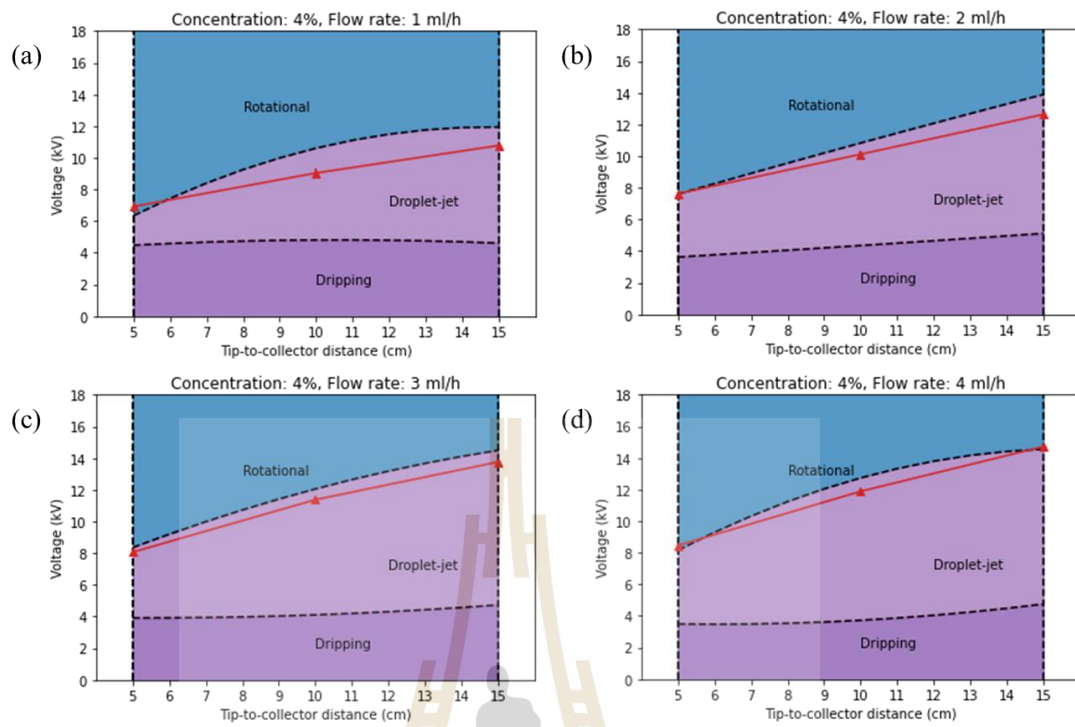


Figure 4.12 Regime map generated of concentration: 4%wt with curve of flow-in rate equal flow-out rate by controlling tip-to-collector distance and voltage at flow rate (a) 1 mL/h, (b) 2 mL/h, (c) 3 mL/h, (d) 4 mL/h.

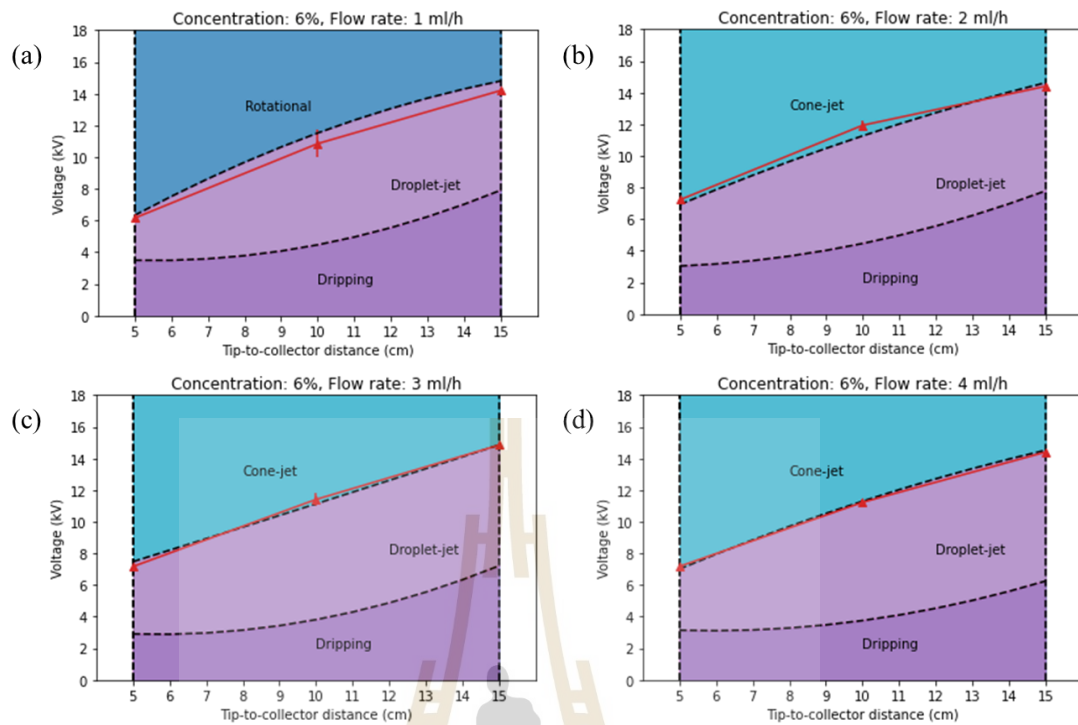


Figure 4.13 Regime map generated of concentration: 6%wt with curve of in rate equal flow-out rate by controlling tip-to-collector distance and voltage at flow rate (a) 1 mL/h, (b) 2 mL/h, (c) 3 mL/h, (d) 4 mL/h.

4.5.3 The regime for fabricated fibers

The regime map and the boundary map of fabricated fibers were combined to form a single map to determine which regimes are suitable for fiber fabrication, as shown in Figures 4.14 to 4.16.

At low concentrations, the solution exhibits low viscosity and low surface tension, which results in the electrospray process, as illustrated in Figure 4.14. This means that a solution with a concentration of 2%wt cannot be used to fabricate fibers in any of the regime maps.

The dripping regime maps in Figures 4.15 and 4.16 appear to show some areas that may be suitable for fiber fabrication. However, this is not accurate as droplet elongation does not occur in the dripping regime. Therefore, fibers should not be produced throughout all areas of the dripping regime map. This issue can be addressed in future research.

A portion of the fabricated fibers with concentrations of 4% wt and 6% wt is found in the droplet-jet regime as shown in Figures 4.15 and 4.16. In addition, with increasing TCD, there is a trend towards fabrication of fibers in the cone-jet regime.

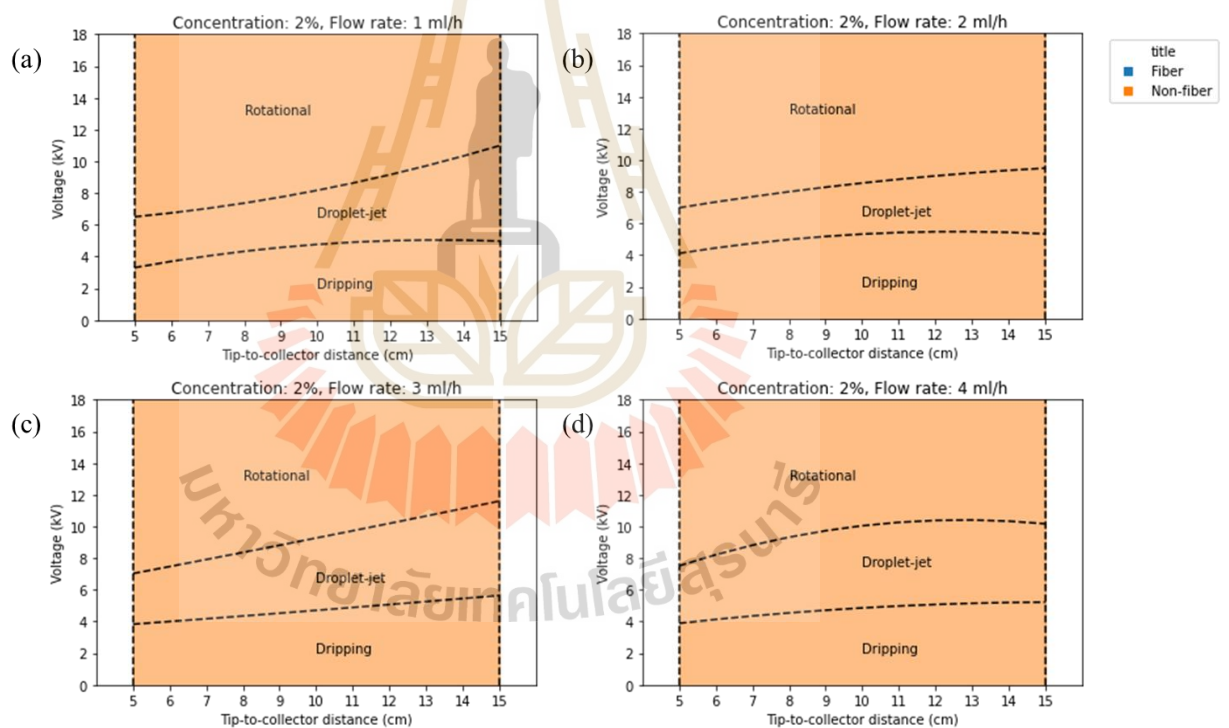


Figure 4.14 Regime map generated of concentration: 2%wt with the boundary map of fabricated fibers by controlling tip-to-collector distance and voltage at flow rate (a) 1 mL/h, (b) 2 mL/h, (c) 3 mL/h, (d) 4 mL/h.

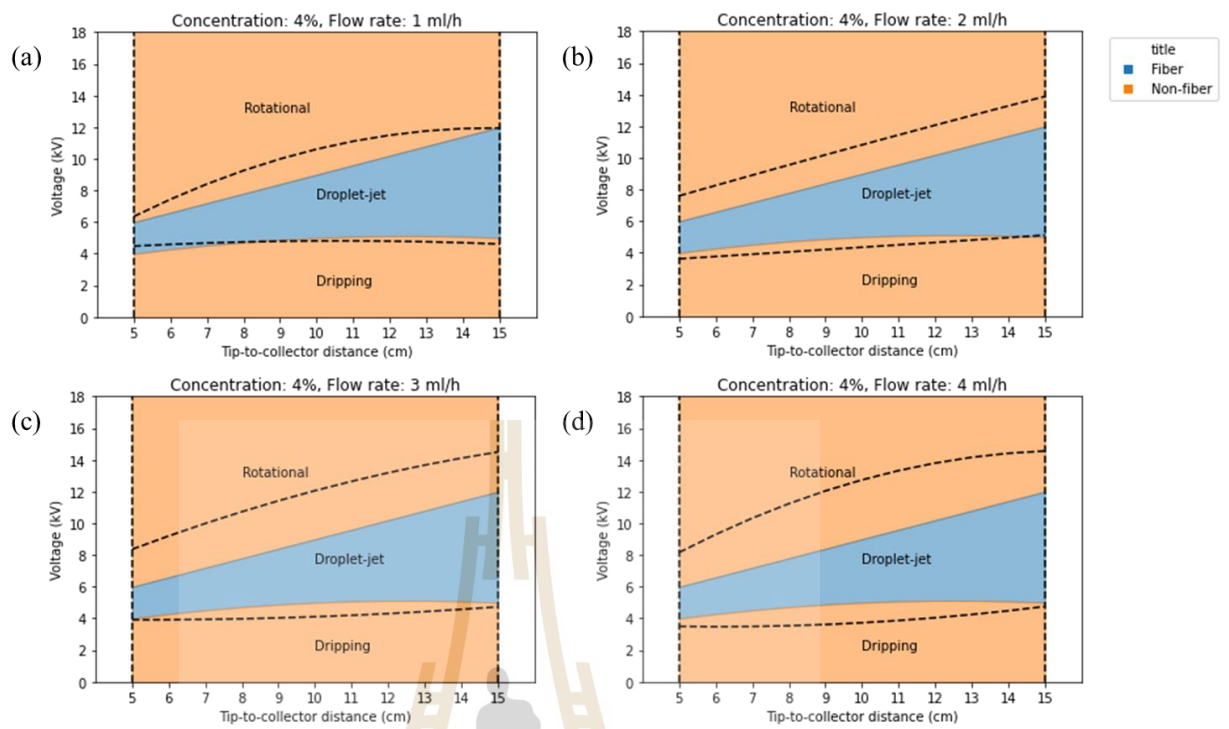


Figure 4.15 Regime map generated of concentration: 4%wt with the boundary map of fabricated fibers by controlling tip-to-collector distance and voltage at flow rate (a) 1 mL/h, (b) 2 mL/h, (c) 3 mL/h, (d) 4 mL/h.

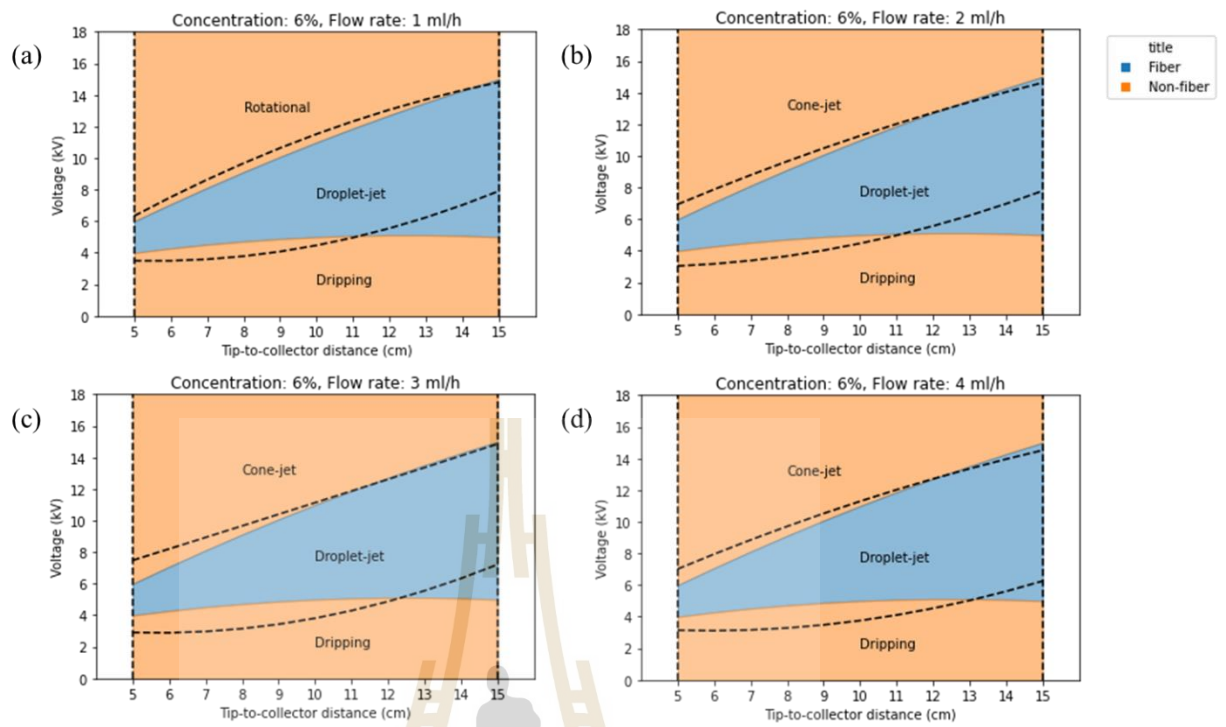


Figure 4.16 Regime map generated of concentration: 6%wt with the boundary map of fabricated fibers by controlling tip-to-collector distance and voltage at flow rate (a) 1 mL/h, (b) 2 mL/h, (c) 3 mL/h, (d) 4 mL/h.

CHAPTER V

CONCLUSIONS

5.1 Conclusions

In this work, stable and continuous fiber productions were studied using deep learning approach, including two implemented models, the object detection and classification models. The purpose of these models was to track the movement and transformation of a jet or Taylor cone and classify the regime of a droplet at the needle tip, respectively.

The object detection model had an average accuracy of about 50%, with a predicted bounding box accuracy of 57.1%, and target detection accuracy of 93.3%. As a result, the F₁ score calculated from the bounding box prediction and target detection was 70.8%. The low accuracy of the model is likely due to the use of low-resolution images in the training process, affecting it difficult to identify objects.

In the classification model, the model was able to categorize four types of regimes with an average accuracy of 90.0%. The correctly predicted cases turned out to be positive cases is 87.2%. While the positives were successfully predicted 92.0%. Thus, the result of F₁ score was 87.1%. Most of the prediction errors occurred in the rotation regime because the limited number of training datasets in this regime and the similar characteristic between rotation and cone-jet systems.

The implemented models can be used to find the correlation of electrospinning parameters. The tracking of the jet transformation revealed a correlation between

voltage and flow rate for continuous fiber production. It was found that when the flow-in rate of the syringe pump is equal to the solution stretching flow-out rate, fiber production is continuous and stable.

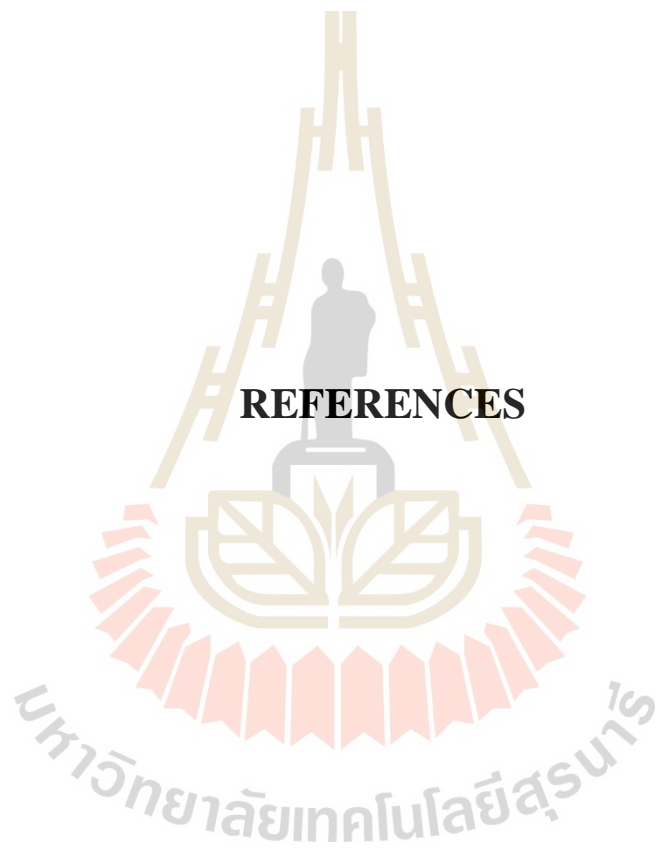
The identification of regimes can categorize the boundaries into four regimes and determine which droplet shape can be continually fabricated. Furthermore, the collecting samples from experiments can help plot the boundary map of fabricated fibers. With all the information mentioned above, it is possible to control continuous fabrication process and understand the boundaries of fiber fabrication.

5.2 Recommendations

The research process was impacted by several issues that were identified during the experiments. The following recommendations are made to address these issues:

- 1) To mitigate the perturbation of the camera caused by the strong electric field generated by the applied high voltage. It is recommended to increase the distance between the camera and the system. This may require the use of a camera with a high-quality telephoto lens.
- 2) The object detection training process was hard to label the object due to the low-resolution image of the dataset (640 x 480). Improving the recording program and using a higher-resolution camera is suggested to resolve this issue.
- 3) The efficiency of the classification model can be improved by increasing the size of the dataset.

REFERENCES



REFERENCES

- Agrahari, V., Agrahari, V., Meng, J., and Mitra, A. K. (2017). Electrospun Nanofibers in Drug Delivery. In **Emerging Nanotechnologies for Diagnostics, Drug Delivery and Medical Devices** (pp. 189-215).
- Alharbi, H. F., Luqman, M., Khalil, K. A., Elnakady, Y. A., Abd-Elkader, O. H., Rady, A. M., Alharthi, N. H., and Karim, M. R. (2018). Fabrication of core-shell structured nanofibers of poly (lactic acid) and poly (vinyl alcohol) by coaxial electrospinning for tissue engineering. **European Polymer Journal**. 98: 483-491.
- Beachley, V., and Wen, X. (2009). Effect of electrospinning parameters on the nanofiber diameter and length. **Mater Sci Eng C Mater Biol Appl**. 29(3): 663-668.
- Brooks, H., and Tucker, N. (2015). Electrospinning predictions using artificial neural networks. **Polymer**. 58: 22-29.
- Camunas-Mesa, L. A., Linares-Barranco, B., and Serrano-Gotarredona, T. (2019). Neuromorphic Spiking Neural Networks and Their Memristor-CMOS Hardware Implementations. **Materials (Basel)**. 12(17).
- Cheng, Z., Cao, J., Kang, L., Luo, Y., Li, T., and Liu, W. (2018). Novel transparent nano-pattern window screen for effective air filtration by electrospinning. **Materials Letters**. 221: 157-160.

- Costa, L. M. M., Bretas, R. E. S., and Gregorio, R. (2010). Effect of Solution Concentration on the Electrospay/Electrospinning Transition and on the Crystalline Phase of PVDF. **Materials Sciences and Applications**. 01(04): 247-252.
- Darrell, H. R., and Iksoo, C. (1996). Nanometre diameter fibres of polymer, produced by electrospinning. **Nanotechnology**. 7(3): 216.
- De Vrieze, S., Van Camp, T., Nelvig, A., Hagström, B., Westbroek, P., and De Clerck, K. (2009). The effect of temperature and humidity on electrospinning. **Journal of Materials Science**. 44(5): 1357-1362.
- Deitzel, J. M., Kleinmeyer, J., Harris, D., and Beck Tan, N. C. (2001). The effect of processing variables on the morphology of electrospun nanofibers and textiles. **Polymer**. 42(1): 261-272.
- Fang, W., Wang, L., and Ren, P. (2020). Tinier-YOLO: A Real-Time Object Detection Method for Constrained Environments. **IEEE Access**. 8: 1935-1944.
- Fernández, A., García, S., Galar, M., Prati, R. C., Krawczyk, B., and Herrera, F. (2018). Learning from Imbalanced Data Sets.
- Filip, P., and Peer, P. (2019). Characterization of Poly(Ethylene Oxide) Nanofibers— Mutual Relations between Mean Diameter of Electrospun Nanofibers and Solution Characteristics. **Processes**. 7(12).
- Garg, K., and Bowlin, G. L. (2011). Electrospinning jets and nanofibrous structures. **Biomicrofluidics**. 5(1): 13403.

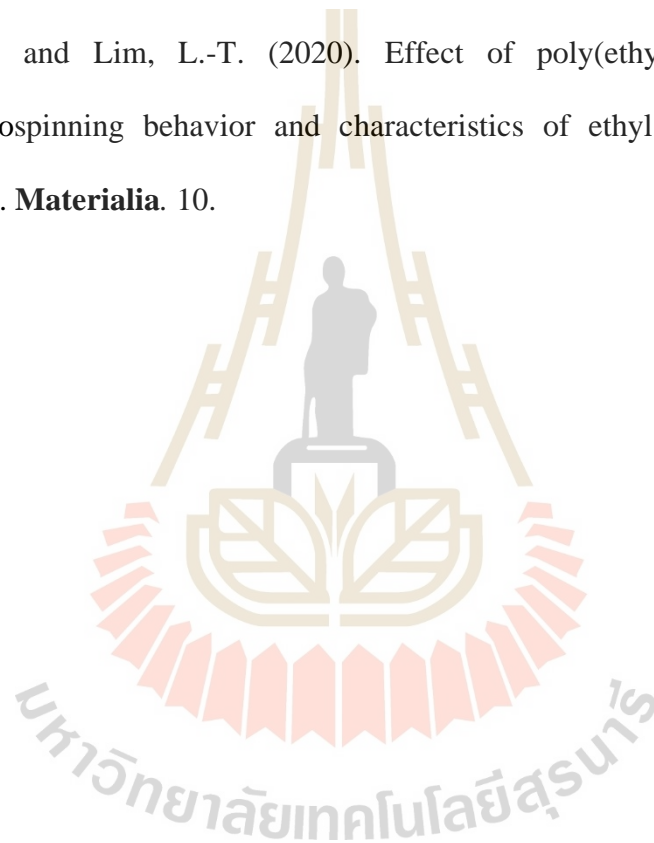
- He, Huang, Wei, Li, and Guo. (2019). TF-YOLO: An Improved Incremental Network for Real-Time Object Detection. **Applied Sciences**. 9(16).
- Hosaini-Alvand, E., Mirshekar, H., Taghi Khorasani, M., Parvazinia, M., and Joorabloo, A. (2017). Fabricating and robust artificial neural network modeling nanoscale polyurethane fiber using electrospinning method. **Journal of Applied Polymer Science**. 134(30).
- Huang, Z.-M., Zhang, Y. Z., Kotaki, M., and Ramakrishna, S. (2003). A review on polymer nanofibers by electrospinning and their applications in nanocomposites. **Composites Science and Technology**. 63(15): 2223-2253.
- Huang, Z.-M., Zhang, Y. Z., Ramakrishna, S., and Lim, C. T. (2004). Electrospinning and mechanical characterization of gelatin nanofibers. **Polymer**. 45(15): 5361-5368.
- Ieracitano, C., Pantò, F., Frontera, P., and Morabito, F. C. (2017). A Neural Network Approach for Predicting the Diameters of Electrospun Polyvinylacetate (PVAc) Nanofibers. In **Engineering Applications of Neural Networks** (pp. 27-38).
- Iregui, A., Irusta, L., Martin, L., and Gonzalez, A. (2019). Analysis of the Process Parameters for Obtaining a Stable Electrospun Process in Different Composition Epoxy/Poly epsilon-Caprolactone Blends with Shape Memory Properties. **Polymers (Basel)**. 11(3).
- Jamshidi, M., and Zilouchian, A. (2001). Intelligent control systems using soft computing methodologies: **CRC press**.

- Joy, N., Anuraj, R., Viravalli, A., Dixit, H. N., and Samavedi, S. (2021). Coupling between voltage and tip-to-collector distance in polymer electrospinning: Insights from analysis of regimes, transitions and cone/jet features. **Chemical Engineering Science**. 230.
- Karakaş, H. (2015). Electrospinning of Nanofibers and Their Applications. **Istanbul Technical University, Textile Technologies and Design Faculty**.
- Karimi, M. A., Pourhakkak, P., Adabi, M., Firoozi, S., Adabi, M., and Naghibzadeh, M. (2015). Using an artificial neural network for the evaluation of the parameters controlling PVA/chitosan electrospun nanofibers diameter. **e-Polymers**. 15(2).
- Khanlou, H. M., Sadollah, A., Ang, B. C., Kim, J. H., Talebian, S., and Ghadimi, A. (2014). Prediction and optimization of electrospinning parameters for polymethyl methacrylate nanofiber fabrication using response surface methodology and artificial neural networks. **Neural Computing and Applications**. 25(3-4): 767-777.
- Khatti, T., Naderi-Manesh, H., and Kalantar, S. M. (2017). Prediction of diameter in blended nanofibers of polycaprolactone-gelatin using ANN and RSM. **Fibers and Polymers**. 18(12): 2368-2378.
- Kulkarni, A., Chong, D., and Batarseh, F. A. (2020). Foundations of data imbalance and solutions for a data democracy. In **Data Democracy** (pp. 83-106).
- Li, D., Wang, Y., and Xia, Y. (2003). Electrospinning of Polymeric and Ceramic Nanofibers as Uniaxially Aligned Arrays. **Nano Letters**. 3(8): 1167-1171.

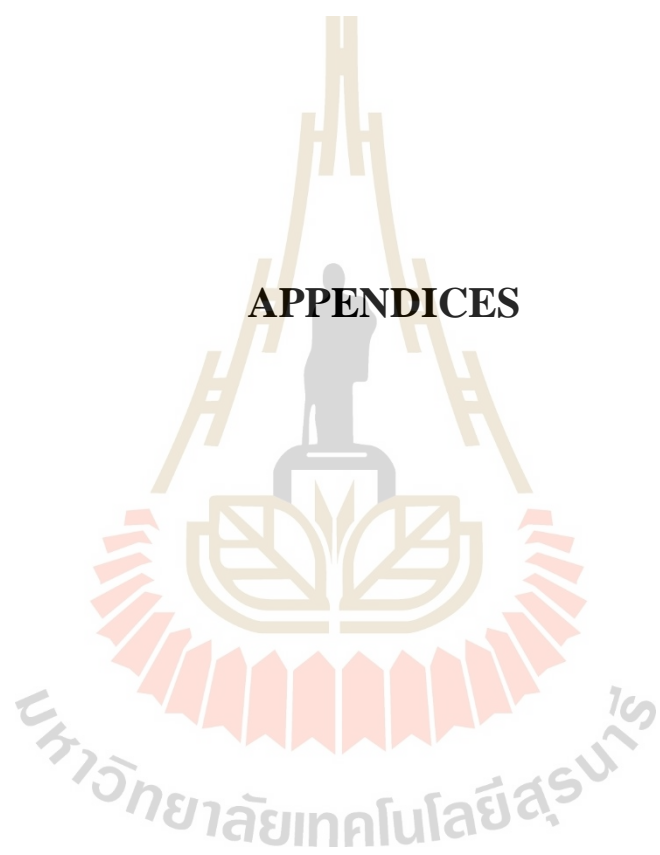
- Li, D., and Xia, Y. (2003). Fabrication of Titania Nanofibers by Electrospinning. **Nano Letters**. 3(4): 555-560.
- Liu, S., and Reneker, D. H. (2019). Droplet-jet shape parameters predict electrospun polymer nanofiber diameter. **Polymer**. 168: 155-158.
- Lou, L., Osemwegie, O., and Ramkumar, S. S. (2020). Functional Nanofibers and Their Applications. **Industrial & Engineering Chemistry Research**. 59(13): 5439-5455.
- Mottaghitlab, V., and Haghi, A. K. (2010). A study on electrospinning of polyacrylonitrile nanofibers. **Korean Journal of Chemical Engineering**. 28(1): 114-118.
- Nasouri, K., Bahrambeygi, H., Rabbi, A., Shoushtari, A. M., and Kafrou, A. (2012). Modeling and optimization of electrospun PAN nanofiber diameter using response surface methodology and artificial neural networks. **Journal of Applied Polymer Science**. 126(1): 127-135.
- Paskiabi, F. A., Mirzaei, E., Amani, A., Shokrgozar, M. A., Saber, R., and Faridi-Majidi, R. (2015). Optimizing parameters on alignment of PCL/PGA nanofibrous scaffold: An artificial neural networks approach. **Int J Biol Macromol**. 81: 1089-1097.
- Rabbi, A., Nasouri, K., Bahrambeygi, H., Shoushtari, A. M., and Babaei, M. R. (2012). RSM and ANN approaches for modeling and optimizing of electrospun polyurethane nanofibers morphology. **Fibers and Polymers**. 13(8): 1007-1014.

- Reneker, D. H., and Yarin, A. L. (2008). Electrospinning jets and polymer nanofibers. **Polymer**. 49(10): 2387-2425.
- Rodríguez-Tobías, H., Morales, G., and Grande, D. (2016). Electrospinning and Electrospaying Techniques for Designing Antimicrobial Polymeric Biocomposite Mats. In **Nanofiber Research - Reaching New Heights**.
- Sarkar, K., Ghalia, M. B., Wu, Z., and Bose, S. C. (2009). A neural network model for the numerical prediction of the diameter of electro-spun polyethylene oxide nanofibers. **Journal of Materials Processing Technology**. 209(7): 3156-3165.
- Sasikala, A. R. K., Unnithan, A. R., Park, C. H., and Kim, C. S. (2019). Nanofiber-based anticancer drug delivery platform. In **Biomimetic Nanoengineered Materials for Advanced Drug Delivery** (pp. 11-36).
- Shin, D., Kim, J., Choi, S., Lee, Y.-b., and Chang, J. (2019). Droplet-jet mode near-field electrospinning for controlled helix patterns with sub-10 μm coiling diameter. **Journal of Micromechanics and Microengineering**. 29(4).
- Sukigara, S., Gandhi, M., Ayutsede, J., Micklus, M., and Ko, F. (2003). Regeneration of Bombyx mori silk by electrospinning—part 1: processing parameters and geometric properties. **Polymer**. 44(19): 5721-5727.
- Xue, J., Wu, T., Dai, Y., and Xia, Y. (2019). Electrospinning and Electrospun Nanofibers: Methods, Materials, and Applications. **Chem Rev**. 119(8): 5298-5415.

- Yang, Y., Jia, Z., Liu, J., Li, Q., Hou, L., Wang, L., and Guan, Z. (2008). Effect of electric field distribution uniformity on electrospinning. **Journal of Applied Physics**. 103(10).
- Yarin, A. L., Koombhongse, S., and Reneker, D. H. (2001). Taylor cone and jetting from liquid droplets in electrospinning of nanofibers. **Journal of Applied Physics**. 90(9): 4836-4846.
- Zaitoon, A., and Lim, L.-T. (2020). Effect of poly(ethylene oxide) on the electrospinning behavior and characteristics of ethyl cellulose composite fibers. **Materialia**. 10.



APPENDICES



APPENDIX A

THE BOUNDARY MAP OF FABRICATED FIBERS

USING SEM FOR THE QUALITY ANALYSIS OF

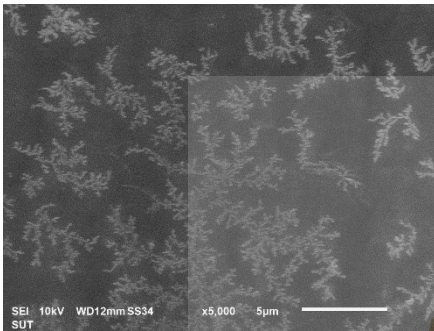
FIBERS

From the results in section III, the boundary map of fabricated fibers, revealed the conditions of the electrospinning parameters that are suitable for fiber fabrication. The process can be outlined as following:

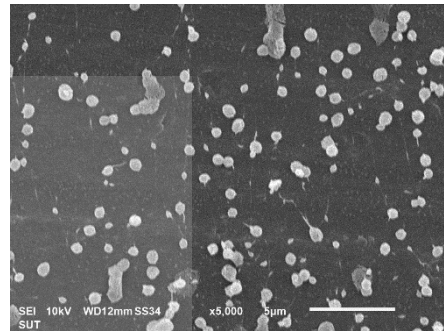
1. Conventional electrospinning with a typical vertical setup was used for all experiments.
2. In each experiment, fiber samples were collected on aluminum foils.
3. The fiber samples were screened by observing if the aluminium foils appeared dry or wet. The results of this screening are presented in Table A.1. In case the aluminium foils appearing wet indicating that the solvents used in some conditions had not completely evaporated.
4. The fiber samples in Table A.1 were analyzed for their morphologies using a scanning electron microscope (SEM).
5. The SEM results were used to determine if the fiber samples could be fabricated by evaluating entire sample. In case all area of the sample was made up of fiber, this will be assumed as able to fabricate fiber. If there

APPENDIX B

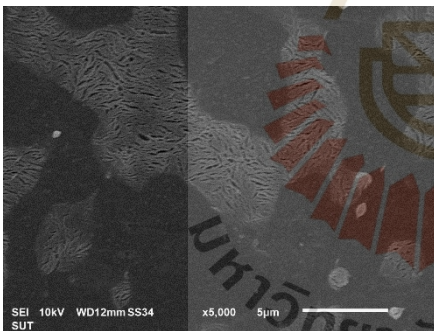
A SAMPLE OF EACH CONDITION



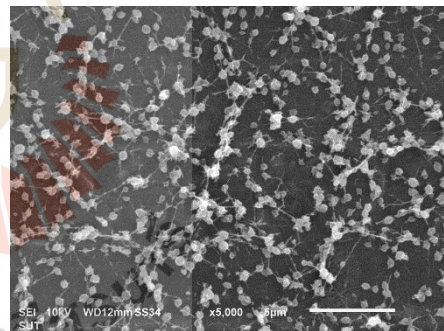
Concentration: 2 % wt, TCD: 5 cm
Flow rate: 1 mL/h, Voltage: 4 kV



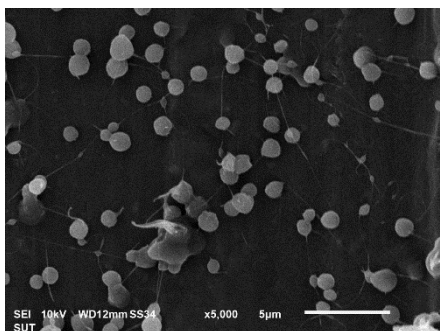
Concentration: 2 % wt, TCD: 5 cm
Flow rate: 1 mL/h, Voltage: 5 kV



Concentration: 2 % wt, TCD: 5 cm
Flow rate: 1 mL/h, Voltage: 6 kV

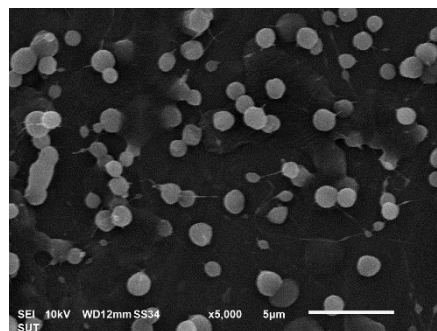


Concentration: 2 % wt, TCD: 10 cm
Flow rate: 1 mL/h, Voltage: 5 kV



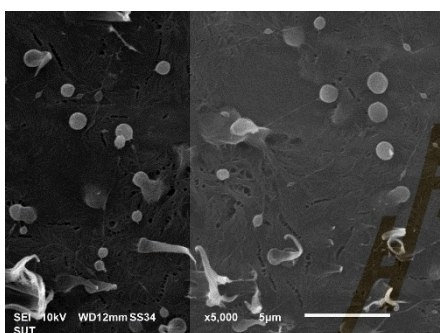
Concentration: 2 % wt, TCD: 10 cm

Flow rate: 1 mL/h, Voltage: 8 kV



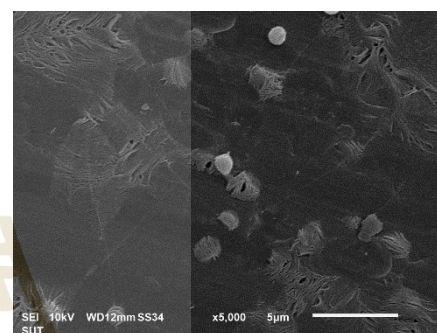
Concentration: 2 % wt, TCD: 10 cm

Flow rate: 2 mL/h, Voltage: 9 kV



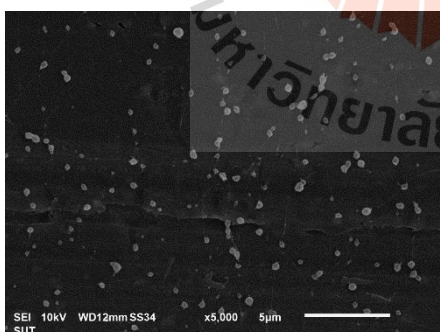
Concentration: 2 % wt, TCD: 10 cm

Flow rate: 3 mL/h, Voltage: 10 kV



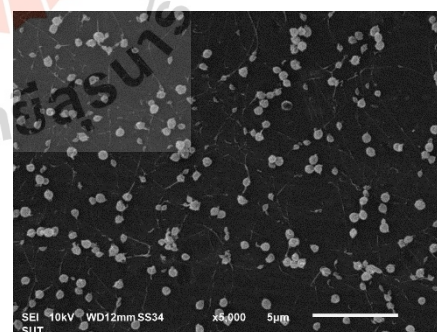
Concentration: 2 % wt, TCD: 10 cm

Flow rate: 4 mL/h, Voltage: 11 kV



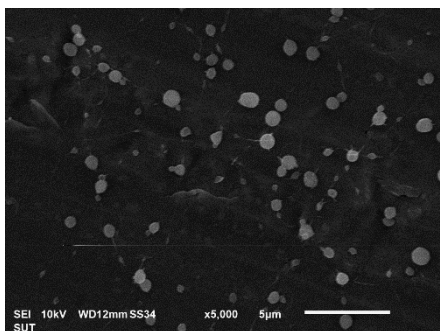
Concentration: 2 % wt, TCD: 15 cm

Flow rate: 1 mL/h, Voltage: 5 kV



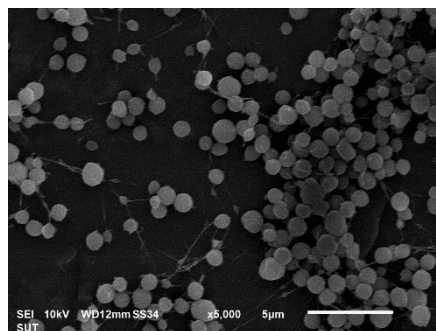
Concentration: 2 % wt, TCD: 15 cm

Flow rate: 1 mL/h, Voltage: 6 kV



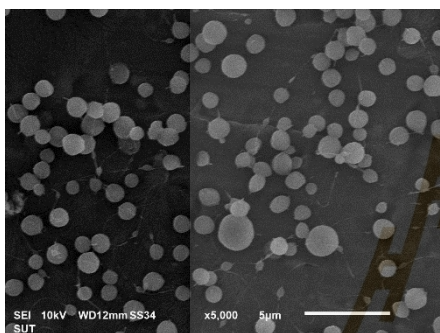
Concentration: 2 % wt, TCD: 15 cm

Flow rate: 1 mL/h, Voltage: 7 kV



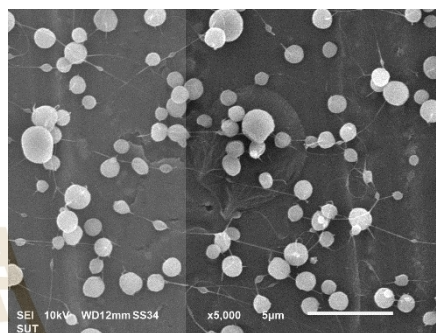
Concentration: 2 % wt, TCD: 15 cm

Flow rate: 1 mL/h, Voltage: 8 kV



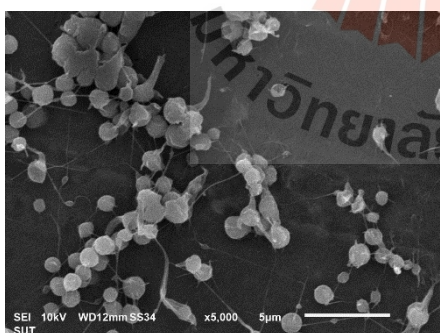
Concentration: 2 % wt, TCD: 15 cm

Flow rate: 1 mL/h, Voltage: 9 kV



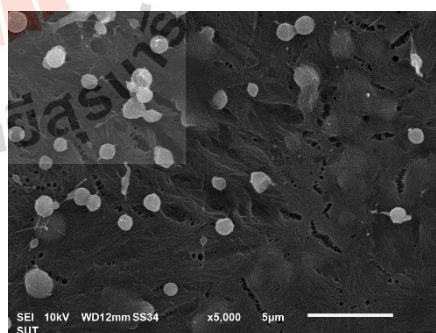
Concentration: 2 % wt, TCD: 15 cm

Flow rate: 2 mL/h, Voltage: 10 kV



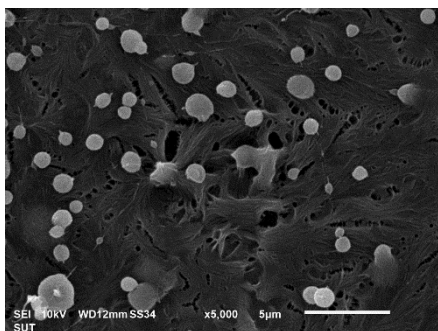
Concentration: 2 % wt, TCD: 15 cm

Flow rate: 3 mL/h, Voltage: 11 kV

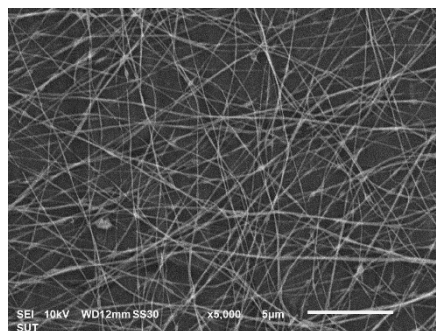


Concentration: 2 % wt, TCD: 15 cm

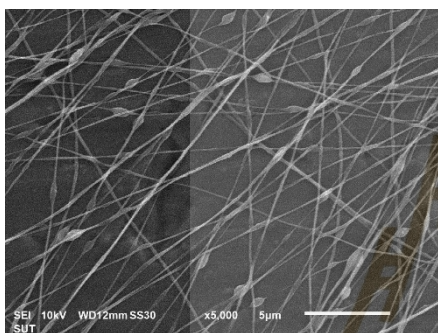
Flow rate: 4 mL/h, Voltage: 12 kV



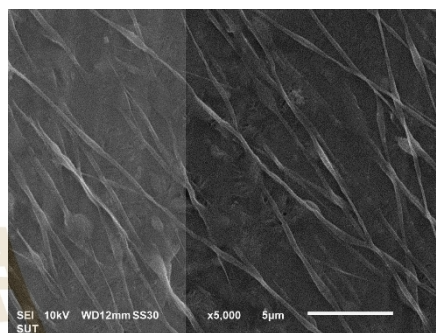
Concentration: 2 % wt, TCD: 15 cm
Flow rate: 4 mL/h, Voltage: 13 kV



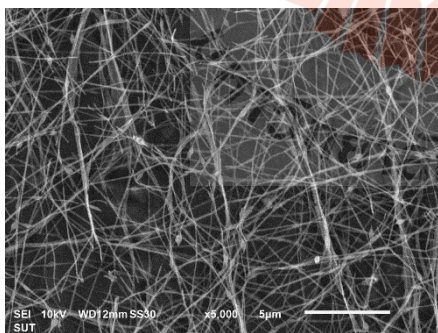
Concentration: 4 % wt, TCD: 5 cm
Flow rate: 1 mL/h, Voltage: 4 kV



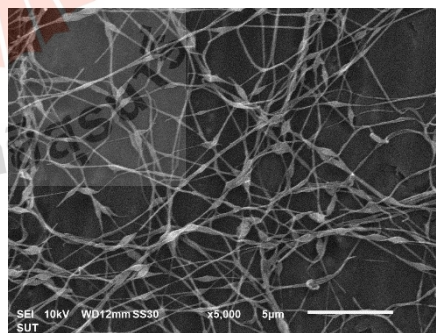
Concentration: 4 % wt, TCD: 5 cm
Flow rate: 1 mL/h, Voltage: 5 kV



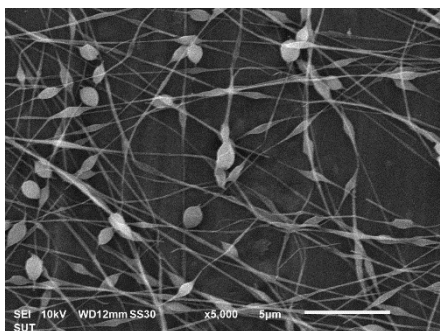
Concentration: 4 % wt, TCD: 5 cm
Flow rate: 1 mL/h, Voltage: 6 kV



Concentration: 4 % wt, TCD: 10 cm
Flow rate: 1 mL/h, Voltage: 4 kV

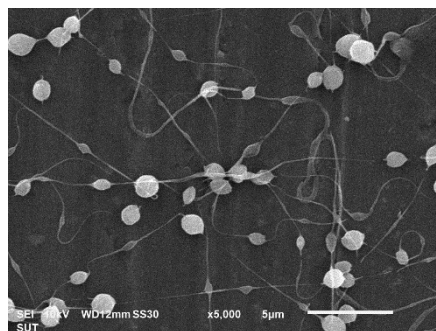


Concentration: 4 % wt, TCD: 10 cm
Flow rate: 1 mL/h, Voltage: 5 kV



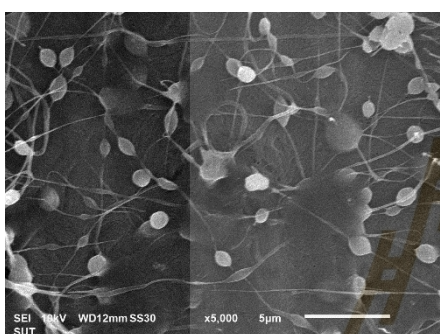
Concentration: 4 % wt, TCD: 10 cm

Flow rate: 1 mL/h, Voltage: 6 kV



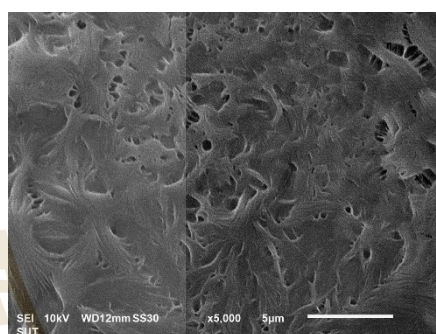
Concentration: 4 % wt, TCD: 10 cm

Flow rate: 1 mL/h, Voltage: 7 kV



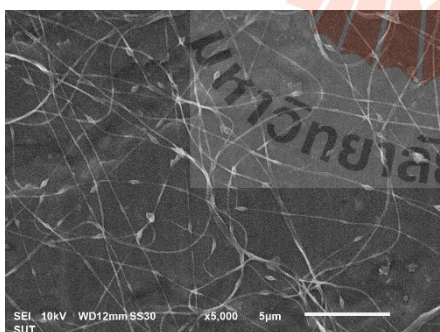
Concentration: 4 % wt, TCD: 10 cm

Flow rate: 2 mL/h, Voltage: 8 kV



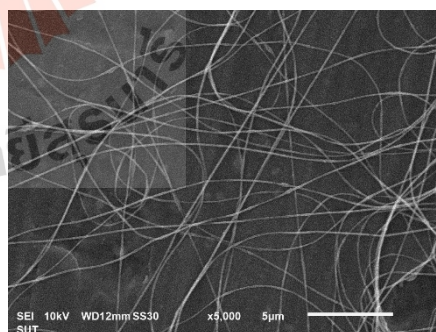
Concentration: 4 % wt, TCD: 10 cm

Flow rate: 1 mL/h, Voltage: 9 kV



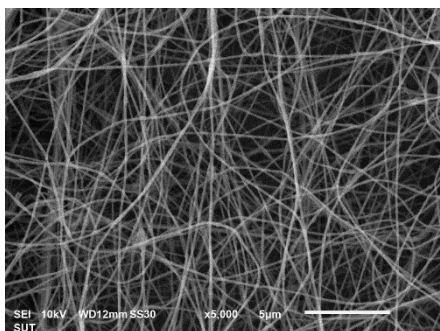
Concentration: 4 % wt, TCD: 15 cm

Flow rate: 1 mL/h, Voltage: 4 kV



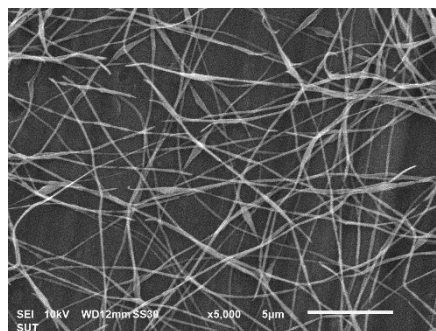
Concentration: 4 % wt, TCD: 15 cm

Flow rate: 1 mL/h, Voltage: 5 kV



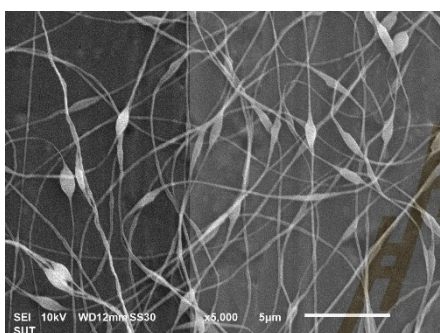
Concentration: 4 % wt, TCD: 15 cm

Flow rate: 1 mL/h, Voltage: 6 kV



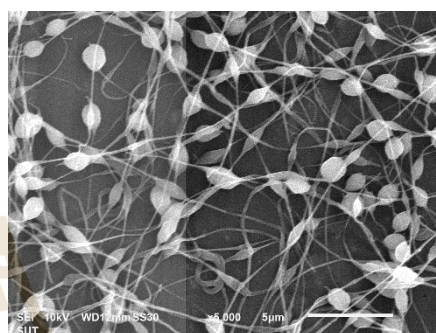
Concentration: 4 % wt, TCD: 15 cm

Flow rate: 1 mL/h, Voltage: 7 kV



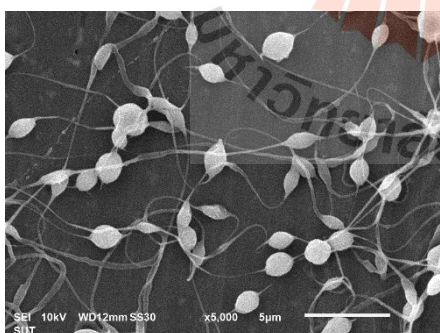
Concentration: 4 % wt, TCD: 15 cm

Flow rate: 1 mL/h, Voltage: 8 kV



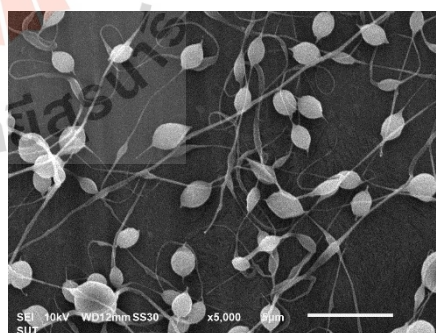
Concentration: 4 % wt, TCD: 15 cm

Flow rate: 1 mL/h, Voltage: 9 kV



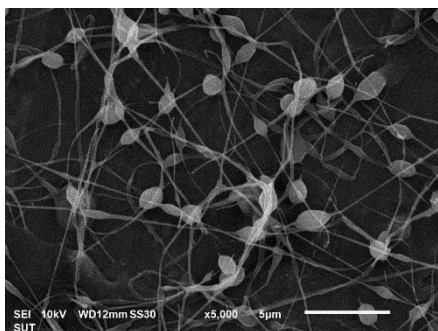
Concentration: 4 % wt, TCD: 15 cm

Flow rate: 2 mL/h, Voltage: 10 kV

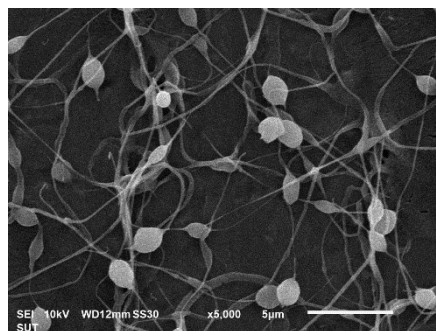


Concentration: 4 % wt, TCD: 15 cm

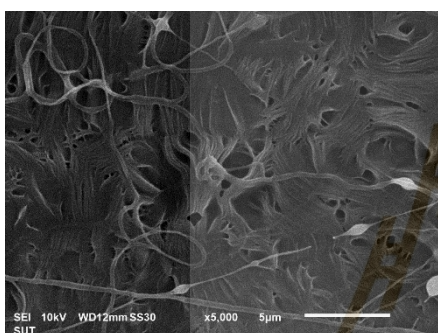
Flow rate: 1 mL/h, Voltage: 11 kV



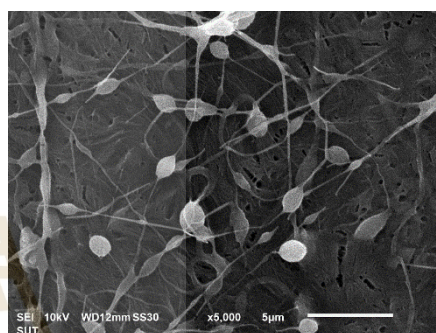
Concentration: 4 % wt, TCD: 15 cm
Flow rate: 2 mL/h, Voltage: 12 kV



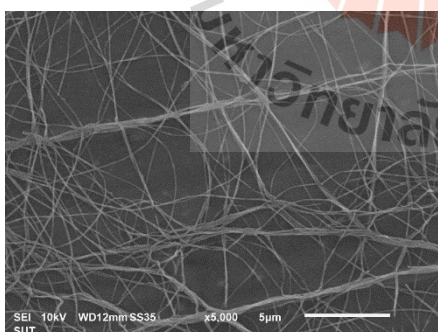
Concentration: 4 % wt, TCD: 15 cm
Flow rate: 3 mL/h, Voltage: 13 kV



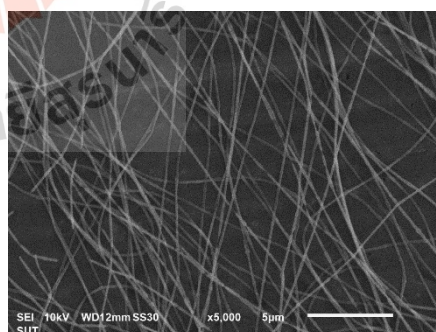
Concentration: 4 % wt, TCD: 15 cm
Flow rate: 4 mL/h, Voltage: 14 kV



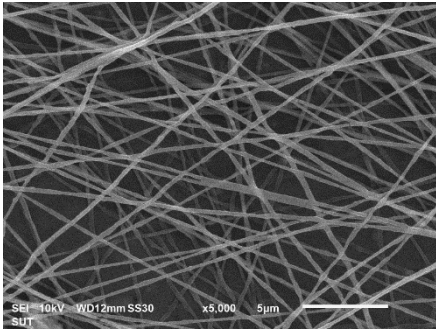
Concentration: 4 % wt, TCD: 15 cm
Flow rate: 4 mL/h, Voltage: 15 kV



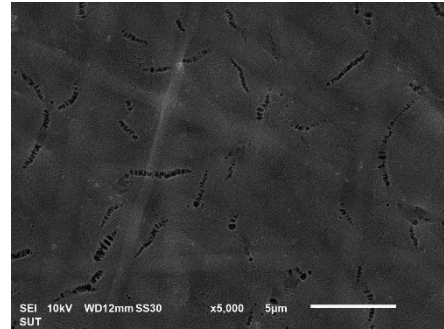
Concentration: 6 % wt, TCD: 5 cm
Flow rate: 1 mL/h, Voltage: 4 kV



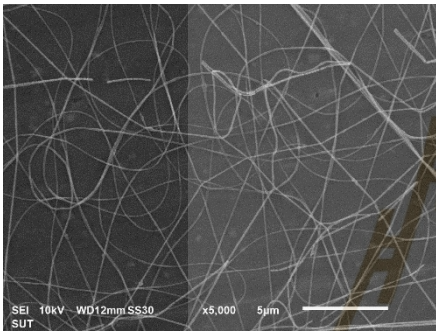
Concentration: 6 % wt, TCD: 5 cm
Flow rate: 1 mL/h, Voltage: 5 kV



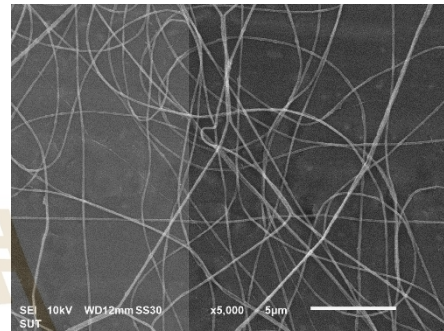
Concentration: 6 % wt, TCD: 5 cm
Flow rate: 1 mL/h, Voltage: 6 kV



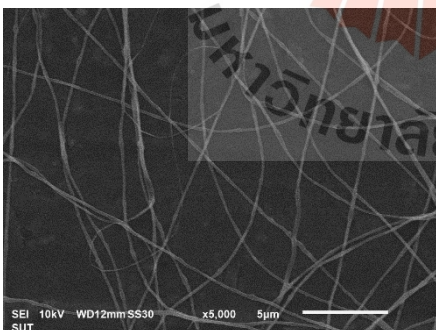
Concentration: 6 % wt, TCD: 5 cm
Flow rate: 1 mL/h, Voltage: 7 kV



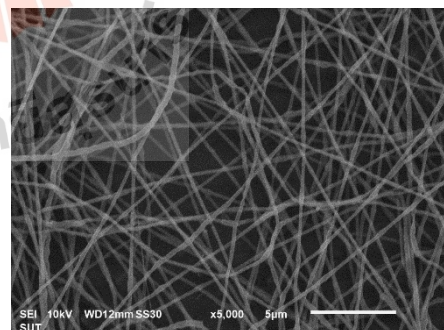
Concentration: 6 % wt, TCD: 10 cm
Flow rate: 1 mL/h, Voltage: 5 kV



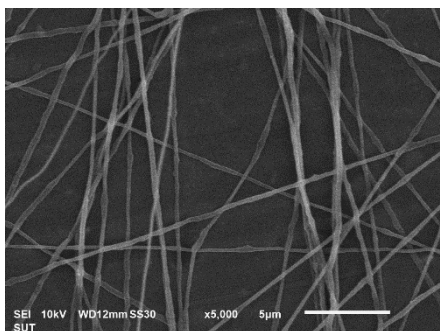
Concentration: 6 % wt, TCD: 10 cm
Flow rate: 1 mL/h, Voltage: 6 kV



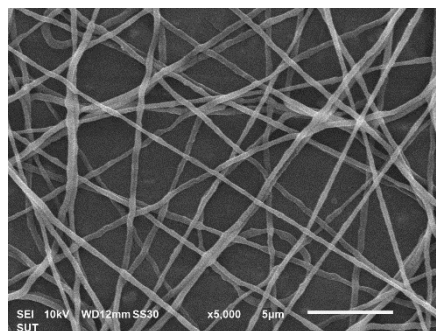
Concentration: 6 % wt, TCD: 10 cm
Flow rate: 1 mL/h, Voltage: 7 kV



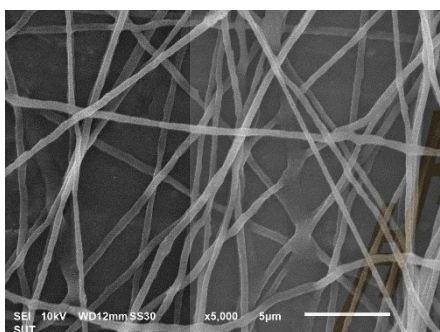
Concentration: 6 % wt, TCD: 10 cm
Flow rate: 1 mL/h, Voltage: 8 kV



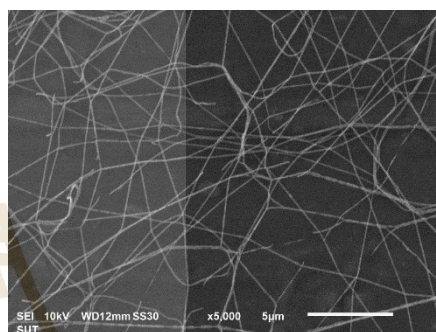
Concentration: 6 % wt, TCD: 10 cm
Flow rate: 1 mL/h, Voltage: 9 kV



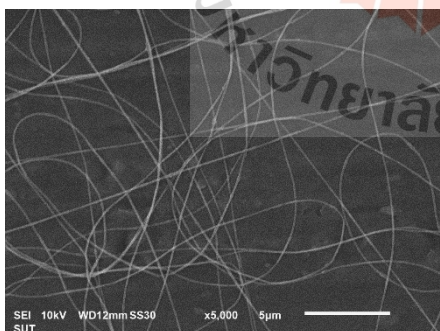
Concentration: 6 % wt, TCD: 10 cm
Flow rate: 1 mL/h, Voltage: 10 kV



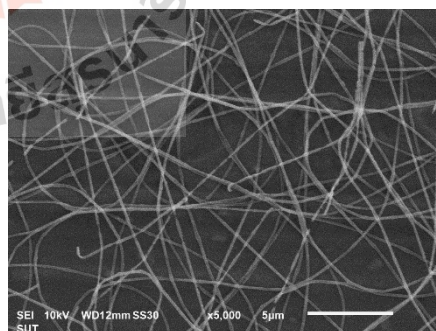
Concentration: 6 % wt, TCD: 10 cm
Flow rate: 1 mL/h, Voltage: 11 kV



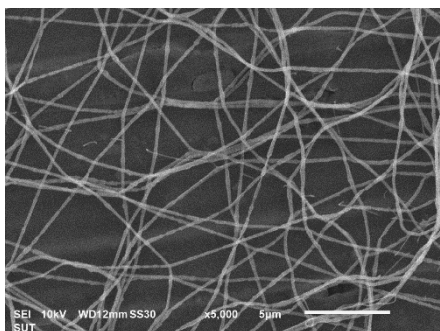
Concentration: 6 % wt, TCD: 15 cm
Flow rate: 1 mL/h, Voltage: 5 kV



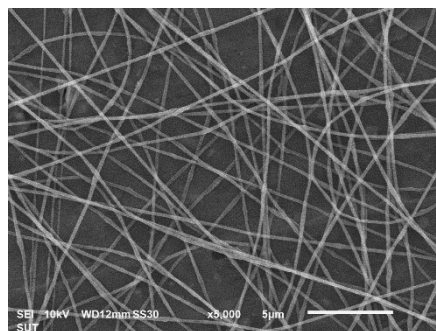
Concentration: 6 % wt, TCD: 15 cm
Flow rate: 1 mL/h, Voltage: 6 kV



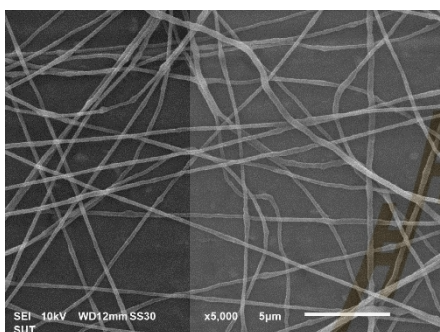
Concentration: 6 % wt, TCD: 15 cm
Flow rate: 1 mL/h, Voltage: 7 kV



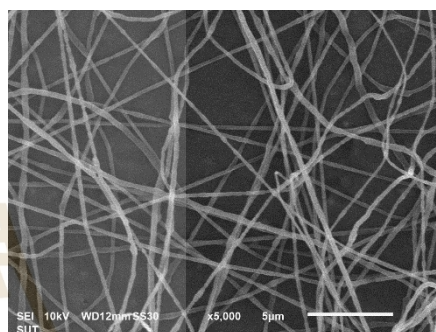
Concentration: 6 % wt, TCD: 15 cm
Flow rate: 1 mL/h, Voltage: 8 kV



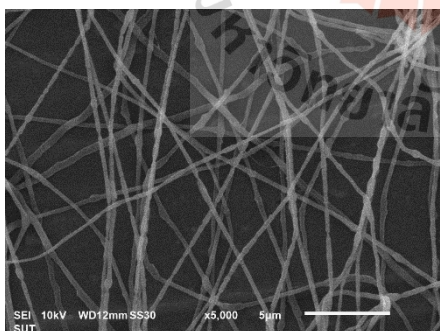
Concentration: 6 % wt, TCD: 15 cm
Flow rate: 1 mL/h, Voltage: 9 kV



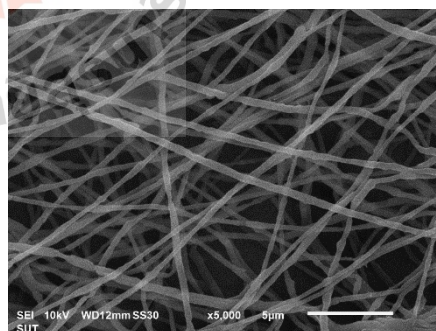
Concentration: 6 % wt, TCD: 15 cm
Flow rate: 1 mL/h, Voltage: 10 kV



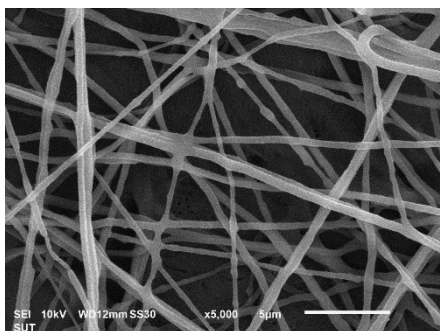
Concentration: 6 % wt, TCD: 15 cm
Flow rate: 1 mL/h, Voltage: 11 kV



Concentration: 6 % wt, TCD: 15 cm
Flow rate: 1 mL/h, Voltage: 12 kV

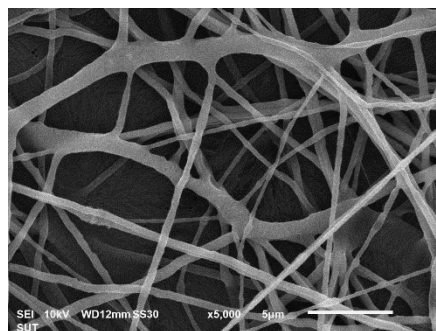


Concentration: 6 % wt, TCD: 15 cm
Flow rate: 1 mL/h, Voltage: 13 kV



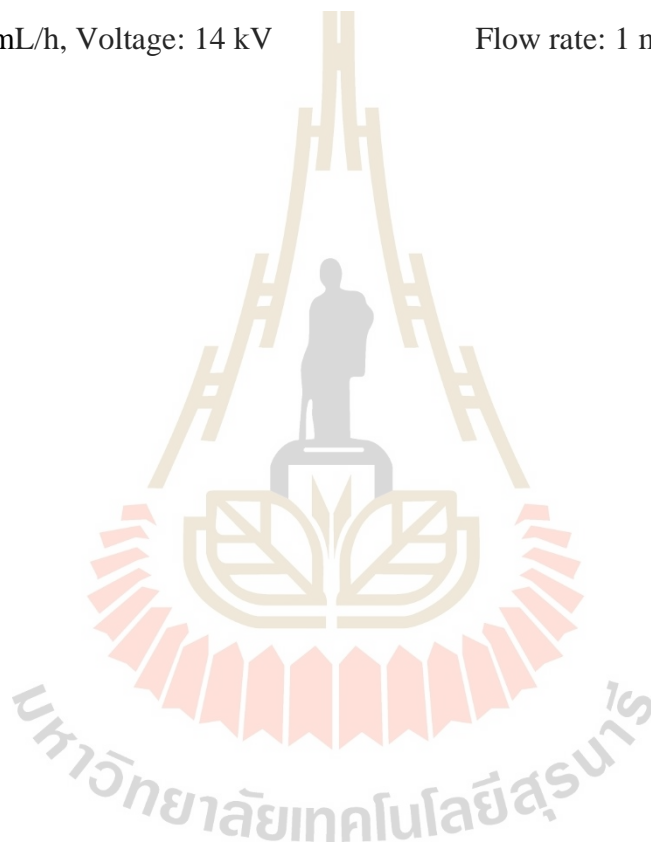
Concentration: 6 % wt, TCD: 15 cm

Flow rate: 1 mL/h, Voltage: 14 kV



Concentration: 6 % wt, TCD: 15 cm

Flow rate: 1 mL/h, Voltage: 15 kV



APPENDIX C

PUBLICATION AND PRESENTATIONS

C.1 List of publication

Soi-ngoen, Y., Fongkaew, I., and Nuansing, W (2021). Prediction of electrospinning parameters for nanofibers production. **In: Proceedings of the IUMRS-ICA 2020 (International Union of Materials Research Societies-International Conference in Asia) [E-Proceeding].**

C.2 List of poster presentation

Soi-ngoen, Y., Fongkaew, I., and Nuansing, W (2021). Prediction of electrospinning parameters for nanofibers production. **The 21st International Union of Materials Research Societies-International Conference in Asia (IUMRS-ICA2020).** Chiang Mai, Thailand.

Prediction of Electrospinning Parameters For Nanofibers Production

Yanawat Soi-ngoen^{1,*}, Ittipon Fongkaew^{1,2}, and Wiwat Nuansing^{1,2,*}

¹School of Physics, Institute of Science, Suranaree University of Technology, Thailand,

²SUT CoE on Advanced Functional Materials (SUT-AFM), Suranaree University of Technology, Thailand

*Corresponding Author's E-mail: yanawat.soi@gmail.com, w.nuansing@g.sut.ac.th

Abstract

Electrospun nanofibers have been widely studied and applied to many applications such as filtration, biomedical membrane, and scaffold in tissue engineering. By controlling the electrospinning parameters, the fibers can be produced from micron- down to nano-diameters. Here we studied influence of the electrospinning parameters to the stability and shape of Taylor cone. The experiments were controlled under 4 % (w/w) polyethylene oxide (PEO) aqueous solution and various conditions including flow rate, tip-to-collector distance (TCD), and voltage (V). The fiber productions were recorded using a video camera with zooming at the the needle tip where the solution is expelled because of the electric force. The experimental results were used for training with a deep learning approach to track and classify the transformation of Taylor cone and the polymer solution jet. The results indicate correlation of flow rate , TCD, and voltage for the stable and continuous fiber production. Moreover, the classification model of PEO solution 4 % (w/w) presents three regimes as dripping, droplet-jet, and rotational. This can be used to predict and determine the scope of the appropriate parameters for continuous fiber production in the industrial scale.

Keywords: Electrospinning, Nanofibers, Taylor Cone, Deep Learning, Polyethylene Oxide

Introduction

Nowadays, fiber or fiber-like materials are used widely in daily life and tend to have more important as they are applied to other fields. Various applications of fibers have been reported in literatures such as biosensor, drug delivery, and tissue engineering [1, 2], where each fiber application needs specific properties of fiber. Fiber production method is one of the most important factor affecting the fiber properties [3]. Study of the fiber production methods can improve the production process and explore new products possibility which may be used further in the applications. Electrospinning technique has been used and studied widely for nanofibers production. This method, an electric force is used as a driving force to transform polymer solution into fiber form [4]. It is an effective technique out of a large-scale process to a low cost, a broadly applicable method for fiber productions on the laboratory and industrial scale [5, 6].

In the electrospinning process, there are many parameters that can affect the process and production quality. To find and learn more about such the stable and continuous fiber production, electrospinning parameters were considered as variants for their involved production. Several studies, for example Joy and co-workers investigated correlations between voltage and TCD with insights of regimes, transitions, and cone-jet shapes [7]. Shin and co-workers studied fabric nanofibers which are produced by the droplet-jet shapes of near-field [8]. Liu analyzed droplet-jet shape and used the results for prediction of nanofiber diameters. In addition, they considered droplet at the tip of the needle and applied the results to control the fiber productions [9]. However, there are many complications and lack of investigations for describing the effect of all parameters on the fiber production in large scale.

Due to various parameters are considered, lots of experimental data and a good analysis method are needed to distinguish the contribution from each parameter. In recent years, deep learning has been applied widely for computer vision applications and research problems. It was designed and

analyzed algorithms that allow machines to establish rules by analyzing data automatically and using them to predict unknown data. This paper aims to study and find a correlation between the electrospinning parameters and fiber production using deep learning models. The electrospinning parameters of this study are flow rate, TCD, and voltage. Two models of object detection and classification model were trained for tracking the transformations of Taylor cone and classifying the regime of droplet by using the deep learning algorithms. We will show here that the deep learning can find the regimes of polymer droplets and predict the conditions of stable and continuous fiber production.

Experimental Procedure

Materials

Polyethylene oxide (PEO, $M_w = 600,000$ g/mol) was purchased from Sigma-Aldrich, USA. The PEO aqueous solutions were prepared by dissolving 4 w/w% of the sample in distilled water separately via a magnetic stirrer (IKA® C-MAG HS hotplate stirrers) at 70 °C for 48 hours.

Electrospinning set-up

A conventional electrospinning set-up as shown in Fig. 1 was constructed and used for all experiments. The electrospinning process was performed at 25 ± 2 °C and relative humidity at 48-52%. PEO aqueous solution was loaded into a 10 mL syringe. A syringe pump (Terumo - Terufusion TE-311 syringe pump) was used to control the flow rate of the PEO solution through a Polyvinyl Chloride (PVC) tube. The PVC tube was connected at one end of the syringe and another with a blunt needle tip (18G, O.D. = 1.27 mm, and I.D. = 0.84 mm). A high voltage power supply (YKY – 50 kV) was used to apply an electric potential by connecting it to the needle. A flat collector with aluminum foil (20 cm x 20 cm) was located under the needle. A video camera (IMSHI 1600X Digital Microscope USB Endoscope Camera) with a backlit light source was introduced to record the electrospinning process at the needle tip.

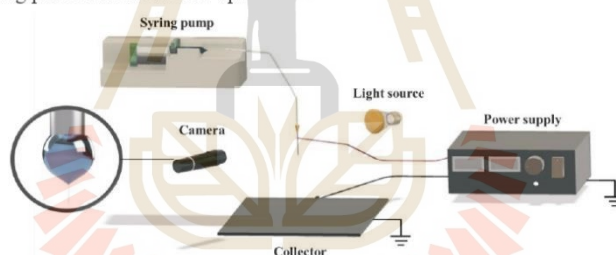


Fig. 1 Schematic diagram of the electrospinning set-up.

Design of experiments

The influence of electrospinning parameters which affecting the fiber production were varied and observed. The experiment parameters consisted of three independent variables as flow rate, TCD, and voltage, similar to other investigations [7, 10]. PEO solution concentration was fixed at 4 % (w/w). Flow rate was set as 1, 2, 3, and 4 ml/h, while TCD was set as 5, 10, and 15 cm. In each condition, TCD and flow rate were identified for every voltage used. The applied voltage was continuously increased from 0 to 15 kV in 2 kV/min increments. The droplet shape was recorded for each condition using the video camera. For each experiment, we repeated the experiment for 4 times in order to obtain 4 datasets. A video dataset was selected as a training dataset and the rest for analytics dataset. The training dataset was used for model training by using the CiRA CORE deep learning software (<https://www.facebook.com/groups/cira.core.comm/>). Two models were trained and tested. First, object detection model was used for tracking of the Taylor cone transformation. Second, classification model was performed for classifying of the polymer solution droplet regime. The

analytics datasets were analyzed by using the models to find a correlation in the electrospinning process.

Object detection model

A droplet at the needle tip was recorded in the electrospinning process (see example in Fig. 2). The videos were extracted to capture frame images in every second. The total images of 634 images were partially randomized and separated for the training 512 images and validating 122 images. The CiRA CORE software was used in this work to label the position information and model training. In the section of target labeling, deep train tool in the software was used for labeling the location of the Taylor cone and bottom curve droplet. Figure 2 shows an example of Taylor cone (TC) labeling and position of the target.

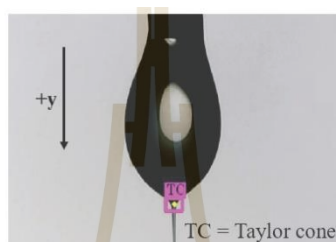


Fig. 2 Taylor cone (TC) labeling and position of the target.

Enhancement methods were used to generate new images in order to extend the dataset. The images were rotated by 90°, 180°, 270° and adjusted contrast 0.4-1.1 by step of 0.1. Figure 3 shows example of the image enhancements. The you-only-look-once (YOLO) algorithm (YOLO v3) is a deep convolutional network structure for object detection. It was used to store the location of Taylor cone in each image. After training the model, the training results were evaluated in a validated dataset of 122 images [11].

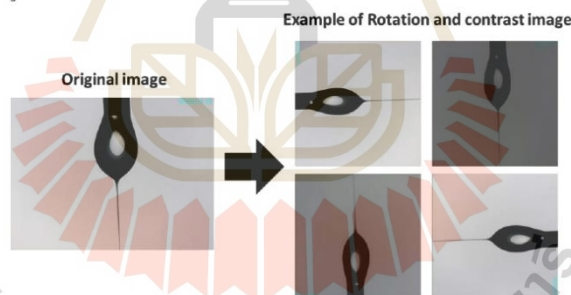


Fig. 3 Enhancement methods by using rotation and contrast enhancement.

Classification model

The datasets were obtained by capturing the experiment videos of all conditions at the needle tip. The datasets consist of four classes such as dripping, droplet-jet, cone-jet, and rotational (see example in Fig. 4). The dripping regime is a droplet shape that the polymer solution droplet can not be elongated as a solution jet because the electric field has not yet reached a critical value. When the electric field is given a critical value that affects the shape of the droplet, the surface of the droplet is elongated by the jet to the collector. This regime is known as the droplet-jet regime. Next, the cone-jet regime is a droplet shape that deforms into the cone and is elongated as a jet. Lastly, the rotational regime is similar to cone-jet regime, but the transformation of Taylor cone has rotational the central

axis of the needle and unstable. In the process, the datasets were randomly selected 664 images consisting of dripping, droplet-jet, cone-jet, and rotational with the image numbers of 200, 200, 200, and 64, respectively. In this model, the enhancement methods were used to generate the images in order to extend the dataset as using in the previous object detection model. Deep train tool in the CiRA CORE was used for training regime of droplets. After training the model, the validated dataset of 166 images were evaluated the model.

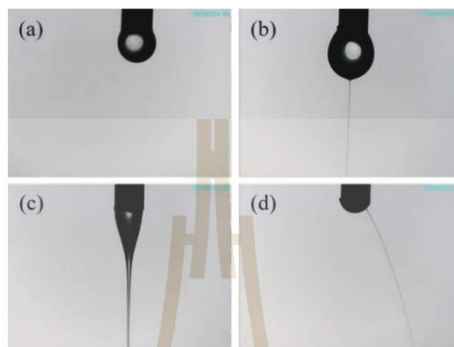


Fig. 4 Example of image data from the training datasets: (a) dripping, (b) droplet-jet, (c) cone-jet, and (d) rotational.

Results and Discussion

Evaluation of object detection model

Implement model for tracking of Taylor cone transformation requires an evaluation to know its effectiveness. The Taylor cone position and the bottom curve droplet were used in all 512 images for the training image. The validation dataset of 122 images were used for the model evaluation. The predicted positions of the validation dataset were plotted comparing with the truth positions. We consider only the y-axis since the droplet expansion is known on the y-axis (see in Fig. 2). It can be plotted a graph between the predicted position of the Taylor cone and truth position on y-axis. Figure 5 presents the comparison result. The graph is a linear regression model, R-squared (R^2) is the measurement that was selected for consideration. The R^2 score of this model is 0.9977, which is high strength of the relationship between predicted and truth position. In addition, there are 5 data from validation dataset that cannot detect Taylor cone, the efficiency of this model is measured by 95.9%. Therefore, this model has good performance.

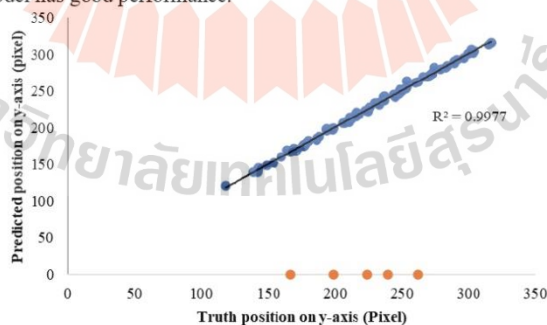


Fig. 5 Comparison between predicted and truth position of Taylor cone on the y-axis.

Evaluation of classification model

Confusion matrix was selected to evaluate this model. Implement model for the classification of the droplet regime, the training dataset contains 664 images categorized into four regimes: dripping, droplet-jet, cone-jet, and rotational, with the images numbers of 200, 200, 200, and 64, respectively. In the validation section, a total of 166 images were used and categorized as 50, 50, 50, 16, respectively. In addition, prediction of the validation dataset was distributed into the confusion matrix as shown in Table 1.

Table 1. Confusion matrix shows prediction of the validation dataset for classification model.

		Actual class			
		Dripping	Droplet-jet	Cone-jet	Rotational
Predicted class	Dripping	50 30.1%	0 0.0%	0 0.0%	0 0.0%
	Droplet-jet	0 0.0%	49 29.5%	0 0.0%	0 0.0%
	Cone-jet	0 0.0%	1 0.6%	35 21.1%	0 0.0%
	Rotational	0 0.0%	0 0.0%	15 9.0%	16 9.6%

The confusion matrix values as shown in Table 2. A total of 216 images are evaluated, a total of 200 images are correctly predicted or 90.4%. In droplet class, it has the highest precision, recall, and F1 score. For droplet-jet and cone-jet class, the predictions are incorrectly images of 1 and 15, respectively. This is due to the class transitions are similar and therefore cross-class predictions are generated. The predicted accuracy is 87.2% and the target is correctly detected by 92.0%. The result of F1 score is 87.1%, which is very accurate prediction of the dripping and droplet-jet class. However, there are about 30% incorrect predictions from the cone-jet class being rotational class because of low numbers of rotational images were used in the model.

Table 2. Summarize the results obtained from the confusion matrix.

Class	Accuracy (%)	Precision (%)	Recall (%)	F1 score (%)
Dripping	90.4	100.0	100.0	100.0
Droplet-jet		100.0	98.0	99.0
Cone-jet		97.2	70.0	81.4
Rotational		51.6	100.0	68.1
Average		87.2	92.0	87.1

Correlations between of flow rate and voltage

The experiment videos were extracted frame images in every second. After that the images were train and tested in both models. Using the object detection model, the extracted images were tracked the Taylor cone position. The position at the top of the image was set to 0 and increased as the position was below the image (see in Fig. 2). The voltage increases by every 2 kV per minute. We can plot graphs between the tracked Taylor cone position on the y-axis and voltage. Figure 6 shows

an example of correlation between the Taylor cone position and voltage (electrospinning process was recorded under flow rate of 1 ml/h and TCD of 5 cm). The correlation graph in Fig. 6 presents first three sharp peaks and the last peak as smooth curve. In the increasing period of Taylor cone position on the y-axis value, this implies to the droplet at the needle tip expanding until the position decrease immediately. This causes the solution droplets at the the needle tip fall down to the collector by gravity force. So, those sharp peaks can refer to the flow-in rate of the polymer solution is more than the flow-out rate. In the section of the last smooth peak, there are three parts would be considered. The ascending slope part indicates the expansion of the droplet, or the flow-in rate is more than the flow-out rate. The descending slope part indicates the droplet is shrinking, or the flow-in rate is less than the flow-out rate. Therefore, the apex part of the last peak can be presented as the flow-in rate equal to the flow-out rate. Moreover, here is a condition that maintains the stability of Taylor cone and continuous fiber production. This is a key important role to control the Taylor cone shapes. To calculate the voltage at the last peak, we generated a polynomial equation of degree six and solved the equation. The solution allows us to know the voltage value at which the flow-in rate is equal to the flow-out rate (optimized parameters) and helps the continuous electrospinning process.

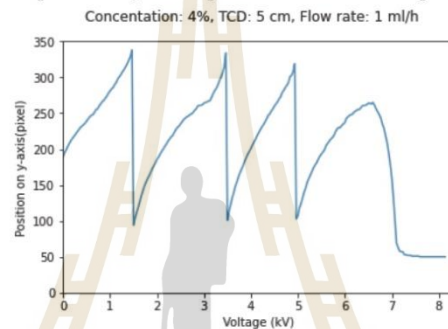


Fig. 6 Example of correlation graph between position of Taylor cone and voltage at TCD of 5 cm and flow rate of 1 ml/h.

From this key result to find an optimized parameter, we know that the TCD and flow rate conditions affecting voltage at the stable Taylor cone shapes. Then adjusting the flow rate and TCD in the electrospinning experiments, we can plot correlation between flow rate and voltage at optimized parameters as shown in Fig. 7. The correlation results show that the voltage must be increase when the TCD values are higher. This is in good agreement with theory of electrospinning process. Thus, it is possible to predict conditions at stable and continuous productions.

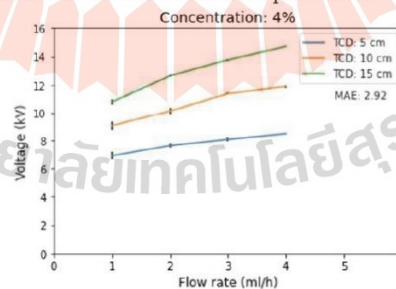


Fig. 7 Correlations between flow rate, voltage, and TCD for the stable Taylor cone shapes.

Identification of regimes

Droplet shapes at the needle tip were classified by classification model and controlling the correlation between voltage and TCD at various flow rates. The results can be boundaries categorized into three regimes: dripping, droplet-jet, and rotational as shown in Fig. 8. The regime mapping of PEO solution with concentration of 4 % (w/w) has no cone-jet regime because the surface tension of the polymer solution is less than the adhesive force between the polymer droplet and the needle tip.

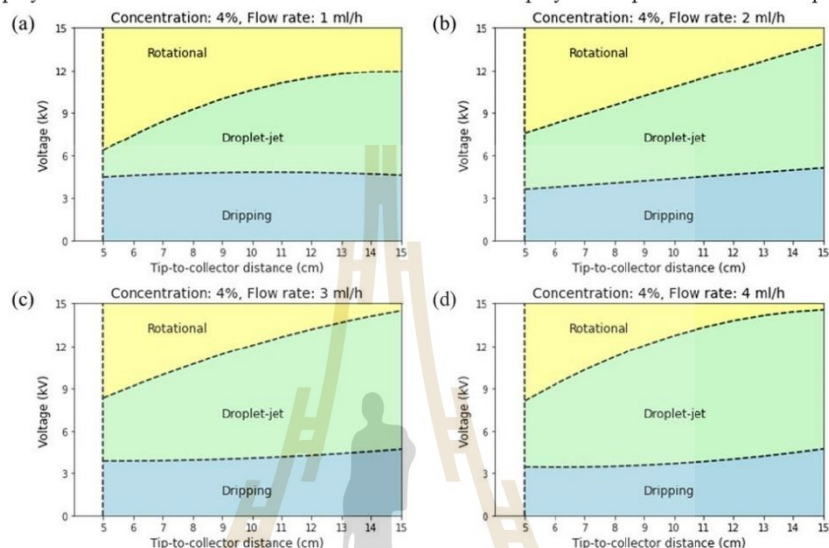


Fig. 8 Regime mapping generated by controlling TCD, voltage, and various flow rate of (a) 1 ml/h, (b) 2 ml/h, (c) 3 ml/h, and (d) 4 ml/h.

Figure 8 shows a clear regime mapping under several electrospinning parameters. However, we found trend of the droplet-jet regime is uncertain because the dripping of solution has a great effect on the initial entry into the droplet-jet regime. So, increasing of flow rate is a method to faster the dripping and speed up the emergence transformation of Taylor cone. This affects the expansion of the droplet-jet regime. In addition, the increasing of TCD value also affects the expansion of the droplet-jet regime.

Conclusions

Taylor cone shapes and electrospinning parameters were studied by using PEO solution with concentration of 4 % (w/w). The implement models can be used to find the correlation of electrospinning parameters. In the part of tracking the Taylor cone transformation, it shows the correlation of voltage and flow rate for the stable and continuous fiber production. The deep learning models used in this work can boundaries categorize four electrospinning regimes. However, PEO solution of 4 % (w/w) can be found only three regimes as dripping, droplet-jet, and rotational. This caused by the surface tension of the polymer solution is less than the adhesive force between the polymer droplet and the needle tip. This can be further improved by increasing of the PEO solution concentration. The correlations between flow rate, voltage, and TCD for the stable Taylor cone shape are in line with theory of electrospinning process. This can be applied to predict and determine the optimized parameters of electrospun nanofibers production in the industrial scale.



Acknowledgments

This research was supported by the Development and Promotion of Science and Technology Talented (DPST), School of Physics, Suranaree University of Technology, and AMP Laboratory.

References

- [1] Agrahari, V., et al., Electrospun Nanofibers in Drug Delivery, in *Emerging Nanotechnologies for Diagnostics, Drug Delivery and Medical Devices*. 2017. p. 189-215.
- [2] Sasikala, A.R.K., et al., Nanofiber-based anticancer drug delivery platform, in *Biomimetic Nanoengineered Materials for Advanced Drug Delivery*. 2019. p. 11-36.
- [3] Lou, L., O. Osemwegie, and S.S. Ramkumar, *Functional Nanofibers and Their Applications*. Industrial & Engineering Chemistry Research, 2020. 59(13): p. 5439-5455.
- [4] Karimi, M.A., et al., Using an artificial neural network for the evaluation of the parameters controlling PVA/chitosan electrospun nanofibers diameter. *e-Polymers*, 2015. 15(2).
- [5] Reneker, D.H. and A.L. Yarin, Electrospinning jets and polymer nanofibers. *Polymer*, 2008. 49(10): p. 2387-2425.
- [6] Nasouri, K., et al., Modeling and optimization of electrospun PAN nanofiber diameter using response surface methodology and artificial neural networks. *Journal of Applied Polymer Science*, 2012. 126(1): p. 127-135.
- [7] Joy, N., et al., Coupling between voltage and tip-to-collector distance in polymer electrospinning: Insights from analysis of regimes, transitions and cone/jet features. *Chemical Engineering Science*, 2021. 230.
- [8] Shin, D., et al., Droplet-jet mode near-field electrospinning for controlled helix patterns with sub-10 μm coiling diameter. *Journal of Micromechanics and Microengineering*, 2019. 29(4).
- [9] Liu, S. and D.H. Reneker, Droplet-jet shape parameters predict electrospun polymer nanofiber diameter. *Polymer*, 2019. 168: p. 155-158.
- [10] Yan, X. and M. Gevelber, Electrospinning of nanofibers: Characterization of jet dynamics and humidity effects. *Particulate Science and Technology*, 2015. 35(2): p. 139-149.
- [11] Xiao, D., et al., A Target Detection Model Based on Improved Tiny-Yolov3 Under the Environment of Mining Truck. *IEEE Access*, 2019. 7: p. 123757-123764.

CURRICULUM VITAE

Name Mr. Yanwarute Soi-ngoen

Date of Birth February 5th, 1995 in Sisaket, Thailand

Place of Birth Thai

E-mail yanawarut soi@gmail.com

Education

2013-2016 B.Sc. (Physics), Khon Kaen University, Thailand

2017-present M.Sc. (Physics), Suranaree University of Technology,
Thailand

Scholarship Development and Promotion of Science and
Technology Talents Project (DPST)

มหาวิทยาลัยเทคโนโลยีสุรนารี